Electronic Supplementary Material (ESI) for Physical Chemistry Chemical Physics.


**Electronic Supplementary Information**

# Mechanism and kinetics of the reaction of Criegee intermediate $CH_2OO$ with acetic acid studied with a time-resolved Fourier-transform IR spectrometer

Bedabyas Behera,[a] Kaito Takahashi*[b] and Yuan-Pern Lee*[ac]

[a]*Department of Applied Chemistry and Institute of Molecular Science, National Yang Ming Chiao Tung University, 1001, Ta-Hsueh Road, Hsinchu 300093, Taiwan.*

[b]*Institute of Atomic and Molecular Science, Academia Sinica, Taipei 106319, Taiwan*

[c]*Center for Emergent Functional Matter Science, National Yang Ming Chiao Tung University, Hsinchu 300093, Taiwan*

Email : kt@gate.sinica.edu.tw; yplee@nycu.edu.tw

## Table of Contents

**A. Computational results**

Geometries of possible reaction intermediates hydroperoxymethyl acetate (HPMA, P1−P5) and hydroxylated secondary ozonide (HSOZ, Q1 and Q2) are presented in Fig. S1. Potential energy scan along the OCOC angle, showing the conversion between conformers of HPMA—P1, P2, and P3, P2 and P4, and P3 and P5—are shown in Figs. S2, S3, and S4, respectively. Geometries of possible pre-reactive complexes (C1 and C2) and end products formic acetic anhydride (FAA, F1−F4) are presented in Fig. S5. Potential energy scan of the conversion among conformers of FAA (F1−F4) is shown in Fig. S6. Geometries of possible transition states are presented in Fig. S7. In Fig. S8, the potential energy curve for the association of $CH_2OO$ and $CH_3C(O)OH$, calculated as a function of the distance between the carbon atom of $CH_2OO$ and the carbonyl oxygen atom of $CH_3C(O)OH$, is given. We summarize different dehydration reaction pathways for conformers P1−P3 of HPMA in Fig. S9.

Harmonic, anharmonic, and scale harmonic vibrational wavenumbers along with their respective infrared (IR) intensities of various conformers of HPMA (P1−P5), HSOZ (Q1 and Q2), and FAA (F1−F4) predicted with the B3LYP/aug-cc-pVTZ method are listed in Tables S1−S3, S4, and S5−S6, respectively. For spectral simulations, the rotational parameters for each vibrational mode of conformers of HPMA, HSOZ, and FAA are presented in Tables S7−S12 (ESI†); the *a*-, *b*-, and *c*-type ratios for each vibrational mode of conformers of HPMA, HSOZ, and FAA are presented in Tables S13−S18 (ESI†).

**B. Simulation of rotational contours of each band**

With program PGopher,[1] we simulated the fundamental band of each vibrational mode of isomers P1−P5 of HPMA and Q1−Q2 of HSOZ in region 800−1800 $cm^{-1}$ using rotational parameters *A*", *B*", and *C*", ratios of rotational parameters *A*'/*A*", *B*'/*B*", and *C*'/*C*" (Tables S7−S10) and the *a*-, *b*-, and *c*-type ratios (Table S13−S16) of each mode predicted with the

B3LYP/aug-cc-pVTZ method, $J_{max}$ = 200, $T$ = 298 K, and Gaussian width 2.6 $cm^{-1}$ (corresponding to the instrument resolution of 2 $cm^{-1}$).

We simulated also the fundamental band of each vibrational mode of isomers F1−F4 of FAA in region 800−1850 $cm^{-1}$ using rotational parameters $A$", $B$", and $C$", ratios of rotational parameters $A'/A$", $B'/B$", and $C'/C$" (Tables S11−S12) and the $a$-, $b$-, and $c$-type ratios (Table S17−18) of each mode predicted with the B3LYP/aug-cc-pVTZ method, $J_{max}$ = 200, $T$ = 298 K, and Gaussian width 2.6 $cm^{-1}$ (corresponding to the instrument resolution of 2 $cm^{-1}$).

**C. Concentration estimation**

The concentration $c$ of the species in our reaction chamber was estimated from its integrated absorbance, $\int A(\nu)d\nu$, and calculated IR band intensity, $S_{band}$, according to the following equation

$$c = \frac{\int A(\nu)d\nu \times ln(10)}{S_{\mathrm{band}} \times L} \qquad \text{(ESI-1)}$$

in which $L$ is the IR absorption length (365 cm), $S_{band}$ is in cm $molecule^{-1}$, and the integrated absorbance is in $cm^{-1}$. For $CH_2I_2$ and $CH_3C(O)OH$, the integrated absorbance in regions 1090−1135 and 1130−1220 $cm^{-1}$, respectively, were used.

We estimated $[CH_2OO]_0$ in the IR-probed volume from the concentration of $[CH_2I]_0$ by assuming that all $CH_2I$ generated after photolysis was converted to $CH_2OO$. We derived the concentration of $[CH_2I]_0$ by probing the decrease in IR absorbance of $CH_2I_2$ ($-\Delta CH_2I_2$) upon photolysis by using Eq. (ESI-1) and assuming the yield to be 1. The band intensity of $CH_2I_2$ in region 1090−1135 $cm^{-1}$ is $1.31\times10^{-17}$ cm $molecule^{-1}$.[2] However, because the IR-probed volume with a path length of 365 cm did not coincide with the photolysis volume in the reactor, the $[CH_2I]_0$ in the photolysis volume was underestimated by a factor. We estimated the volume ratio $V_{IR}/V_{photolysis}$, in which $V_{IR}$ is the IR-probed volume and $V_{photolysis}$ is the UV-photolysis volume, from the measured $-\Delta CH_2I_2$, hence $[CH_2OO]_0$ in the IR-probed volume, as discussed

above, and the $[CH_2OO]_0$ in the photolysis volume from the kinetic fitting of the $CH_2I + O_2$ system,[3,4] to be discussed below.

We performed similar experiments without $CH_3C(O)OH$ and fitted the temporal profiles of $CH_2OO$ with the established model,[5] listed in Table S20, except that the reaction $CH_2OO + CH_3C(O)OH$ was excluded from the model. The experimental conditions of 8 experiments in 2 sets are listed in Table S19. The temporal profiles of $CH_2OO$ were obtained on integrating region 905−915 $cm^{-1}$. These profiles were then fitted with the kinetics model by varying $[CH_2OO]_0$ to derive the best fit. Representative temporal profiles of $CH_2OO$ with their fitted curves are shown in Fig. S12. This fitted $[CH_2OO]_0$ in the photolysis volume was compared with the $[CH_2OO]_0$ in the IR-probed volume to derive $V_{IR}/V_{photolysis}$. The resultant volume ratio $V_{IR}/V_{photolysis}$ from experiments at various pressures are presented in Fig. S13; the average value is 3.5 ± 0.11. In experiments of $CH_2OO + CH_3C(O)OH$, we obtained the $[CH_2OO]_0$ in the photolysis volume, which is the value to use in kinetic modeling, by multiplying the volume ratio $V_{IR}/V_{photolysis}$ with the loss of the IR-probed $[CH_2I_2]$ upon photolysis.

**D. Kinetics model to fit the reaction $CH_2OO + CH_3C(O)OH$**

The rate coefficient of the $CH_2OO + CH_3C(O)OH \rightarrow$ HPMA reaction was obtained by fitting the production profiles of HPMA or by fitting the decay profiles of $CH_2OO$. We fitted the temporal profile by a kinetics model similar to that employed for fitting the $CH_2OO + HC(O)OH \rightarrow$ HPMF reaction,[4] except that the fitted reaction is changed to $CH_2OO + CH_3C(O)OH \rightarrow$ HPMA, as listed in Table S20. The self-reaction of $CH_2OO$ and other secondary reactions were taken into account in the model. Because the experiments were performed under a limited pressure range, we simplified the pressure-dependent rate coefficients of $CH_2I + O_2$, $k_1$*–$k_3$*, to constant values.

The initial concentrations of $CH_2I_2$ and $CH_3C(O)OH$ in the reactor were determined from the integrated absorbance in regions 1090−1135 and 1130−1220 $cm^{-1}$, respectively, by the

method described in Section C; reported IR intensities $1.31\times10^{-17}$ and $3.12\times10^{-17}$cm molecule$^{-1}$ for $CH_2I_2$[2] and $CH_3C(O)OH$,[6] respectively, were used. The initial concentration of $CH_2I$ in the IR-probed volume was estimated from $-\Delta[CH_2I_2]$ upon irradiation. The initial concentration of $CH_2I$, in the photolysis volume, $[CH_2I]_0$, was consequently estimated by $-(V_{IR}/V_{photolysis}) \times \Delta[CH_2I_2] = -3.5 \times \Delta[CH_2I_2]$, as discussed in Section C. We also estimated the $[CH_2I]_0$ in the photolysis volume from the photolysis yield of $CH_2I_2$ by the equation,

$$[CH_2I]_0 = y \times [CH_2I_2]_0, \quad (2)$$

in which $y$ was the fraction of $CH_2I_2$ that was photolyzed. The value of $y$ was obtained from $(F/h\nu_{308}) \times \sigma_{308}$, in which $F$ is the laser fluence and $\sigma_{308}$ is the absorption cross-section of $CH_2I_2$ at 308 nm, which is $3.2\times10^{-18}$ cm$^2$ molecule$^{-14}$.[7] The deviation of these two estimates are typically within ±40 %. For example, in experiment no. 1 the value of $[CH_2I]_0$ obtained from the decay of $CH_2I_2$ was $3.5\times6.3\times10^{13} = 2.2\times10^{14}$ molecule cm$^{-3}$, whereas with a laser fluence of 65 mJ cm$^{-2}$, $y$ = 0.32 and $[CH_2I]_0$ was $0.32\times9.8\times10^{14} = 3.1\times10^{14}$ molecule cm$^{-3}$. For the model fitting, we used the $[CH_2OO]_0$ values estimated from volume ratio $V_{IR}/V_{photolysis}$ and the loss of $CH_2I_2$; values estimated according to the laser fluence were only used as estimates of errors.

Representative temporal profiles of production of HPMA and curves fitted with the kinetics model are presented in Fig. 8 of the main text. Representative experimental temporal profiles of $CH_2OO$ and curves fitted with the kinetics model are presented in Fig. S14. A summary of experimental conditions and the fitted results ($k^I$) are listed in Table S21. A plot of the first-order rate coefficient in the 31 experiments obtained from the production of HPMA is shown in Fig. 9a of the main text. We obtained a bimolecular rate coefficient of $(1.32 \pm 0.04)\times10^{-10}$ cm$^3$ molecules$^{-1}$ s$^{-1}$. A plot of the first-order rate coefficient in the experiment set 3 obtained from $CH_2OO$ fitting is shown in Fig. 9b of the main text, with a bimolecular rate

coefficient of $(1.26 \pm 0.06)\times10^{-10}$ $cm^3$ $molecules^{-1}$ $s^{-1}$, consistent with that derived from the formation of HPMA. Error analysis is discussed in the main text.

**Table S1** Harmonic, anharmonic, and scaled harmonic vibrational wavenumbers ($cm^{-1}$) and IR intensities (km $mol^{-1}$, listed parenthetically) of conformers P1 and P2 of hydroperoxymethyl acetate (HPMA) predicted with the B3LYP/aug-cc-pVTZ method

| Mode | P1 | | | P2 | | |
|---|---|---|---|---|---|---|
| | Harmonic | Anharmonic | Scaled harmonic[a] | Harmonic | Anharmonic | Scaled harmonic[a] |
| $\nu_1$ | 3499 (311) | 3290 (274) | | 3746 (33) | 3576 (22) | |
| $\nu_2$ | 3159 (4) | 3022 (3) | | 3157 (5) | 3020 (6) | |
| $\nu_3$ | 3141 (4) | 2992 (7) | | 3149 (4) | 3003 (12) | |
| $\nu_4$ | 3111 (2) | 2979 (2) | | 3109 (4) | 2987 (4) | |
| $\nu_5$ | 3071 (20) | 2951 (19) | | 3081 (23) | 2959 (21) | |
| $\nu_6$ | 3053 (1) | 2952 (1) | | 3052 (1) | 2949 (1) | |
| $\nu_7$ | 1760 (251) | 1715 (174) | 1726 (251) | 1808 (263) | 1774 (140) | 1773 (263) |
| $\nu_8$ | 1499 (96) | 1443 (70) | 1471 (96) | 1478 (9) | 1439 (5) | 1450 (9) |
| $\nu_9$ | 1477 (8) | 1434 (5) | 1450 (8) | 1470 (16) | 1435 (8) | 1443 (16) |
| $\nu_{10}$ | 1472 (14) | 1436 (17) | 1444 (14) | 1465 (13) | 1431 (9) | 1438 (13) |
| $\nu_{11}$ | 1469 (25) | 1427 (29) | 1442 (25) | 1422 (20) | 1406 (37) | 1396 (20) |
| $\nu_{12}$ | 1425 (35) | 1414 (21) | 1398 (35) | 1399 (29) | 1346 (30) | 1374 (29) |
| $\nu_{13}$ | 1401 (22) | 1354 (2) | 1375 (22) | 1375 (53) | 1339 (14) | 1350 (53) |
| $\nu_{14}$ | 1310 (5) | 1276 (1) | 1286 (5) | 1318 (1) | 1270 (10) | 1294 (1) |
| $\nu_{15}$ | 1264 (256) | 1225 (219) | 1242 (256) | 1229 (310) | 1196 (151) | 1208 (310) |
| $\nu_{16}$ | 1154 (22) | 1131 (22) | 1135 (22) | 1164 (13) | 1144 (8) | 1144 (13) |
| $\nu_{17}$ | 1085 (47) | 1061 (17) | 1067 (47) | 1069 (9) | 1045 (6) | 1051 (9) |
| $\nu_{18}$ | 1072 (6) | 1043 (6) | 1055 (6) | 1058 (26) | 1053 (52) | 1041 (26) |
| $\nu_{19}$ | 1029 (116) | 996 (45) | 1012 (116) | 1019 (220) | 983 (25) | 1003 (220) |
| $\nu_{20}$ | 956 (98) | 917 (109) | 941 (98) | 970 (147) | 927 (253) | 955 (147) |
| $\nu_{21}$ | 881 (68) | 855 (79) | 868 (68) | 883 (36) | 862 (55) | 870 (36) |
| $\nu_{22}$ | 824 (29) | 805 (25) | 812 (29) | 839 (16) | 822 (9) | 827 (16) |
| $\nu_{23}$ | 692 (0) | 679 (1) | 683 (0) | 668 (7) | 664 (6) | 660 (7) |
| $\nu_{24}$ | 631 (72) | 740 (3) | 624 (72) | 615 (8) | 619 (1) | 608 (8) |
| $\nu_{25}$ | 597 (37) | 387 (52) | 590 (37) | 563 (5) | 549 (10) | 558 (5) |
| $\nu_{26}$ | 541 (21) | 536 (20) | 536 (21) | 472 (31) | 460 (27) | 469 (31) |
| $\nu_{27}$ | 460 (5) | 455 (2) | 457 (5) | 364 (8) | 363 (7) | 363 (8) |
| $\nu_{28}$ | 363 (5) | 354 (3) | 362 (5) | 277 (16) | 223 (38) | 278 (16) |
| $\nu_{29}$ | 233 (11) | 235 (10) | 236 (11) | 219 (108) | 402 (31) | 222 (108) |
| $\nu_{30}$ | 212 (11) | 187 (12) | 214 (11) | 148 (4) | 185 (44) | 153 (4) |
| $\nu_{31}$ | 134 (3) | 121 (3) | 139 (3) | 96 (0) | 55 (1) | 102 (0) |
| $\nu_{32}$ | 93 (1) | 81 (0) | 99 (1) | 63 (0) | 143 (2) | 70 (0) |
| $\nu_{33}$ | 52 (0) | 60 (0) | 59 (0) | 43 (1) | 90 (8) | 50 (1) |

[a] Harmonic vibrational wavenumber scaled according to $0.9761\ x + 7.9$, in which $x$ is the harmonic vibrational wavenumber; this equation is only valid for wavenumbers below 2000 $cm^{-1}$.

**Table S2** Harmonic, anharmonic, and scaled harmonic vibrational wavenumbers ($cm^{-1}$) and IR intensities (km $mol^{-1}$, listed parenthetically) of conformers P3 and P4 of hydroperoxymethyl acetate (HPMA) predicted with the B3LYP/aug-cc-pVTZ method

| Mode | P3 | | | P4 | | |
|---|---|---|---|---|---|---|
| | Harmonic | Anharmonic | Scaled harmonic[a] | Harmonic | Anharmonic | Scaled harmonic[a] |
| $\nu_1$ | 3739 (37) | 3549 (28) | | 3728 (34) | 3541 (26) | |
| $\nu_2$ | 3156 (5) | 3011 (6) | | 3157 (3) | 3021 (2) | |
| $\nu_3$ | 3126 (8) | 2974 (14) | | 3134 (7) | 2990 (12) | |
| $\nu_4$ | 3109 (4) | 2975 (2) | | 3106 (2) | 2980 (3) | |
| $\nu_5$ | 3064 (12) | 2946 (9) | | 3071 (23) | 2965 (14) | |
| $\nu_6$ | 3051 (1) | 2928 (5) | | 3046 (1) | 2935 (5) | |
| $\nu_7$ | 1787 (274) | 1776 (244) | 1753 (274) | 1825 (336) | 1786 (285) | 1789 (336) |
| $\nu_8$ | 1482 (7) | 1431 (2) | 1455 (7) | 1495 (7) | 1453 (8) | 1467 (7) |
| $\nu_9$ | 1478 (8) | 1444 (7) | 1451 (8) | 1489 (8) | 1443 (3) | 1462 (8) |
| $\nu_{10}$ | 1472 (15) | 1436 (12) | 1444 (15) | 1469 (17) | 1423 (13) | 1442 (17) |
| $\nu_{11}$ | 1419 (19) | 1395 (20) | 1393 (19) | 1415 (9) | 1383 (10) | 1389 (9) |
| $\nu_{12}$ | 1398 (41) | 1322 (3) | 1372 (41) | 1399 (34) | 1369 (38) | 1373 (34) |
| $\nu_{13}$ | 1379 (43) | 1353 (53) | 1354 (43) | 1385 (60) | 1344 (13) | 1360 (60) |
| $\nu_{14}$ | 1284 (6) | 1236 (6) | 1261 (6) | 1308 (18) | 1274 (14) | 1285 (18) |
| $\nu_{15}$ | 1256 (353) | 1204 (214) | 1234 (353) | 1225 (254) | 1192 (122) | 1204 (254) |
| $\nu_{16}$ | 1144 (43) | 1110 (37) | 1124 (43) | 1143 (24) | 1116 (2) | 1123 (24) |
| $\nu_{17}$ | 1090 (24) | 1065 (16) | 1072 (24) | 1069 (91) | 1041 (26) | 1051 (91) |
| $\nu_{18}$ | 1069 (6) | 1048 (5) | 1052 (6) | 1061 (64) | 1036 (62) | 1044 (64) |
| $\nu_{19}$ | 1033 (228) | 1013 (109) | 1016 (228) | 1031 (79) | 999 (49) | 1014 (79) |
| $\nu_{20}$ | 958 (62) | 915 (164) | 943 (62) | 986 (175) | 958 (203) | 971 (175) |
| $\nu_{21}$ | 939 (39) | 898 (108) | 925 (39) | 881 (27) | 857 (25) | 868 (27) |
| $\nu_{22}$ | 882 (23) | 859 (36) | 868 (23) | 784 (11) | 766 (11) | 773 (11) |
| $\nu_{23}$ | 636 (3) | 621 (1) | 629 (3) | 663 (27) | 652 (13) | 656 (27) |
| $\nu_{24}$ | 606 (6) | 598 (4) | 600 (6) | 576 (7) | 569 (5) | 570 (7) |
| $\nu_{25}$ | 554 (1) | 541 (0) | 549 (1) | 529 (13) | 522 (10) | 525 (13) |
| $\nu_{26}$ | 440 (21) | 434 (13) | 438 (21) | 485 (4) | 478 (5) | 481 (4) |
| $\nu_{27}$ | 358 (7) | 333 (10) | 358 (7) | 420 (3) | 416 (3) | 418 (3) |
| $\nu_{28}$ | 270 (121) | 105 (17) | 272 (121) | 291 (47) | 254 (60) | 292 (47) |
| $\nu_{29}$ | 219 (22) | 246 (11) | 221 (22) | 247 (61) | 195 (54) | 249 (61) |
| $\nu_{30}$ | 168 (5) | 135 (106) | 172 (5) | 185 (0) | 216 (32) | 188 (0) |
| $\nu_{31}$ | 102 (1) | 57 (3) | 107 (1) | 156 (13) | 106 (2) | 160 (13) |
| $\nu_{32}$ | 58 (0) | 25 (0) | 64 (0) | 79 (1) | 62 (7) | 85 (1) |
| $\nu_{33}$ | 34 (2) | -76 (33) | 41 (2) | 63 (9) | 49 (8) | 70 (9) |

[a] Harmonic vibrational wavenumber scaled according to $0.9761\ x + 7.9$, in which $x$ is the harmonic vibrational wavenumber; this equation is only valid for wavenumbers below 2000 $cm^{-1}$.

**Table S3** Harmonic, anharmonic, and scaled harmonic vibrational wavenumbers ($cm^{-1}$) and IR intensities (km $mol^{-1}$, listed parenthetically) of conformer P5 of hydroperoxymethyl acetate (HPMA) predicted with the B3LYP/aug-cc-pVTZ method

| Mode | P5 | | |
|---|---|---|---|
| | Harmonic | Anharmonic | Scaled harmonic[a] |
| $\nu_1$ | 3746 (53) | 3568 (42) | |
| $\nu_2$ | 3156 (3) | 3019 (3) | |
| $\nu_3$ | 3127 (11) | 2979 (8) | |
| $\nu_4$ | 3111 (2) | 2984 (2) | |
| $\nu_5$ | 3070 (24) | 2964 (12) | |
| $\nu_6$ | 3049 (1) | 2933 (10) | |
| $\nu_7$ | 1820 (339) | 1781 (281) | 1785 (339) |
| $\nu_8$ | 1499 (1) | 1454 (2) | 1471 (1) |
| $\nu_9$ | 1487 (11) | 1444 (10) | 1459 (11) |
| $\nu_{10}$ | 1472 (12) | 1424 (4) | 1445 (12) |
| $\nu_{11}$ | 1417 (17) | 1387 (8) | 1391 (17) |
| $\nu_{12}$ | 1398 (45) | 1364 (24) | 1372 (45) |
| $\nu_{13}$ | 1381 (35) | 1345 (24) | 1356 (35) |
| $\nu_{14}$ | 1313 (23) | 1271 (8) | 1290 (23) |
| $\nu_{15}$ | 1216 (281) | 1180 (168) | 1195 (281) |
| $\nu_{16}$ | 1149 (1) | 1124 (2) | 1129 (1) |
| $\nu_{17}$ | 1078 (120) | 1047 (86) | 1060 (120) |
| $\nu_{18}$ | 1061 (25) | 1036 (41) | 1044 (25) |
| $\nu_{19}$ | 1029 (104) | 997 (76) | 1012 (104) |
| $\nu_{20}$ | 996 (131) | 970 (184) | 980 (131) |
| $\nu_{21}$ | 881 (33) | 858 (33) | 867 (33) |
| $\nu_{22}$ | 803 (7) | 787 (6) | 791 (7) |
| $\nu_{23}$ | 631 (32) | 621 (32) | 624 (32) |
| $\nu_{24}$ | 576 (4) | 567 (3) | 570 (4) |
| $\nu_{25}$ | 517 (8) | 509 (7) | 513 (8) |
| $\nu_{26}$ | 479 (1) | 478 (1) | 476 (1) |
| $\nu_{27}$ | 395 (12) | 387 (9) | 393 (12) |
| $\nu_{28}$ | 307 (32) | 475 (9) | 308 (32) |
| $\nu_{29}$ | 275 (91) | 43 (23) | 277 (91) |
| $\nu_{30}$ | 193 (0) | 208 (5) | 196 (0) |
| $\nu_{31}$ | 157 (7) | 123 (8) | 161 (7) |
| $\nu_{32}$ | 81 (4) | 68 (6) | 87 (4) |
| $\nu_{33}$ | 59 (7) | 31 (2) | 66 (7) |

[a] Harmonic vibrational wavenumber scaled according to $0.9761\ x + 7.9$, in which $x$ is the harmonic vibrational wavenumber; this equation is only valid for wavenumbers below 2000 $cm^{-1}$.

**Table S4** Harmonic, anharmonic, and scaled harmonic vibrational wavenumbers ($cm^{-1}$) and intensities (km $mol^{-1}$, listed parenthetically) of conformers Q1 and Q2 of hydroxylated secondary ozonide (HSOZ) predicted with the B3LYP/aug-cc-pVTZ method

| Mode | Q1 | | | Q2 | | |
|---|---|---|---|---|---|---|
| | Harmonic | Anharmonic | Scaled harmonic[a] | Harmonic | Anharmonic | Scaled harmonic[a] |
| $\nu_1$ | 3784 (43) | 3602 (36) | | 3802 (44) | 3636 (40) | |
| $\nu_2$ | 3148 (8) | 3016 (7) | | 3143 (7) | 3005 (9) | |
| $\nu_3$ | 3138 (5) | 3001 (7) | | 3123 (9) | 3012 (8) | |
| $\nu_4$ | 3106 (13) | 2962 (18) | | 3103 (14) | 2959 (18) | |
| $\nu_5$ | 3065 (4) | 2956 (5) | | 3054 (6) | 2937 (8) | |
| $\nu_6$ | 3010 (69) | 2857 (53) | | 3007 (76) | 2855 (45) | |
| $\nu_7$ | 1522 (1) | 1482 (1) | 1494 (1) | 1525 (0) | 1484 (1) | 1496 (0) |
| $\nu_8$ | 1490 (1) | 1447 (1) | 1462 (1) | 1492 (2) | 1452 (1) | 1464 (2) |
| $\nu_9$ | 1483 (3) | 1440 (1) | 1455 (3) | 1484 (2) | 1446 (2) | 1456 (2) |
| $\nu_{10}$ | 1436 (61) | 1393 (40) | 1410 (61) | 1416 (35) | 1384 (42) | 1390 (35) |
| $\nu_{11}$ | 1397 (15) | 1367 (14) | 1372 (15) | 1410 (12) | 1380 (8) | 1384 (12) |
| $\nu_{12}$ | 1384 (38) | 1339 (3) | 1359 (38) | 1332 (67) | 1278 (23) | 1308 (67) |
| $\nu_{13}$ | 1234 (9) | 1200 (12) | 1212 (9) | 1238 (32) | 1206 (32) | 1216 (32) |
| $\nu_{14}$ | 1213 (251) | 1173 (100) | 1192 (251) | 1198 (50) | 1166 (28) | 1177 (50) |
| $\nu_{15}$ | 1159 (12) | 1140 (23) | 1139 (12) | 1176 (240) | 1159 (64) | 1156 (240) |
| $\nu_{16}$ | 1141 (57) | 1106 (39) | 1121 (57) | 1149 (14) | 1122 (8) | 1129 (14) |
| $\nu_{17}$ | 1099 (74) | 1077 (49) | 1081 (74) | 1100 (94) | 1070 (26) | 1082 (94) |
| $\nu_{18}$ | 1070 (130) | 1034 (102) | 1052 (130) | 1080 (110) | 1045 (98) | 1062 (110) |
| $\nu_{19}$ | 982 (63) | 948 (70) | 966 (63) | 988 (53) | 951 (61) | 972 (53) |
| $\nu_{20}$ | 965 (72) | 944 (70) | 950 (72) | 956 (74) | 933 (78) | 941 (74) |
| $\nu_{21}$ | 891 (9) | 870 (6) | 878 (9) | 893 (2) | 870 (3) | 880 (2) |
| $\nu_{22}$ | 846 (30) | 824 (26) | 834 (30) | 873 (26) | 853 (21) | 860 (26) |
| $\nu_{23}$ | 816 (15) | 798 (12) | 804 (15) | 830 (3) | 813 (3) | 818 (3) |
| $\nu_{24}$ | 730 (7) | 716 (7) | 720 (7) | 731 (4) | 718 (3) | 721 (4) |
| $\nu_{25}$ | 656 (5) | 647 (5) | 648 (5) | 656 (3) | 646 (2) | 648 (3) |
| $\nu_{26}$ | 564 (14) | 553 (13) | 559 (14) | 570 (14) | 561 (10) | 565 (14) |
| $\nu_{27}$ | 515 (13) | 504 (8) | 511 (13) | 509 (7) | 505 (7) | 504 (7) |
| $\nu_{28}$ | 379 (12) | 374 (32) | 378 (12) | 376 (6) | 347 (2) | 375 (6) |
| $\nu_{29}$ | 369 (41) | 362 (13) | 368 (41) | 346 (13) | 316 (19) | 346 (13) |
| $\nu_{30}$ | 331 (30) | 314 (12) | 331 (30) | 279 (16) | 408 (3) | 280 (16) |
| $\nu_{31}$ | 259 (21) | 233 (60) | 261 (21) | 226 (88) | 71 (34) | 228 (88) |
| $\nu_{32}$ | 193 (3) | 191 (1) | 196 (3) | 212 (2) | 210 (36) | 215 (2) |
| $\nu_{33}$ | 114 (3) | 93 (1) | 119 (3) | 115 (12) | 107 (11) | 120 (12) |

[a] Harmonic vibrational wavenumber scaled according to $0.9761\ x + 7.9$, in which $x$ is the harmonic vibrational wavenumber; this equation is only valid for wavenumbers below 2000 $cm^{-1}$.

**Table S5** Harmonic, anharmonic, and scaled harmonic vibrational wavenumbers ($cm^{-1}$) and IR intensities (km $mol^{-1}$, listed parenthetically) of conformers F1 and F2 of formic acetic anhydride (FAA) predicted with the B3LYP/aug-cc-pVTZ method

| Mode | F1 | | | F2 | | |
|---|---|---|---|---|---|---|
| | Harmonic | Anharmonic | Scaled harmonic[a] | Harmonic | Anharmonic | Scaled harmonic[a] |
| $\nu_1$ | 3160 (4) | 3013 (5) | | 3158 (4) | 3009 (5) | |
| $\nu_2$ | 3109 (1) | 2964 (2) | | 3108 (2) | 2967 (1) | |
| $\nu_3$ | 3084 (9) | 2935 (11) | | 3049 (0) | 2926 (1) | |
| $\nu_4$ | 3052 (0) | 2941 (0) | | 3038 (48) | 2892 (50) | |
| $\nu_5$ | 1849 (211) | 1825 (118) | 1813 (211) | 1885 (351) | 1848 (331) | 1848 (351) |
| $\nu_6$ | 1824 (379) | 1787 (341) | 1788 (379) | 1802 (169) | 1772 (82) | 1766 (169) |
| $\nu_7$ | 1474 (9) | 1422 (5) | 1446 (9) | 1475 (9) | 1439 (6) | 1448 (9) |
| $\nu_8$ | 1468 (16) | 1429 (14) | 1441 (16) | 1468 (14) | 1431 (13) | 1441 (14) |
| $\nu_9$ | 1404 (50) | 1368 (46) | 1378 (50) | 1403 (22) | 1374 (34) | 1377 (22) |
| $\nu_{10}$ | 1381 (1) | 1351 (1) | 1356 (1) | 1400 (15) | 1359 (1) | 1375 (15) |
| $\nu_{11}$ | 1202 (289) | 1174 (145) | 1181 (289) | 1174 (122) | 1141 (64) | 1154 (122) |
| $\nu_{12}$ | 1069 (7) | 1044 (1) | 1051 (7) | 1084 (500) | 1060 (59) | 1066 (500) |
| $\nu_{13}$ | 1057 (594) | 1026 (491) | 1039 (594) | 1068 (133) | 1034 (410) | 1051 (133) |
| $\nu_{14}$ | 1047 (0) | 1027 (0) | 1030 (0) | 1026 (42) | 1009 (37) | 1009 (42) |
| $\nu_{15}$ | 995 (10) | 972 (81) | 980 (10) | 1007 (117) | 980 (315) | 991 (117) |
| $\nu_{16}$ | 938 (106) | 916 (128) | 923 (106) | 795 (32) | 779 (22) | 784 (32) |
| $\nu_{17}$ | 639 (9) | 628 (8) | 632 (9) | 750 (34) | 732 (58) | 740 (34) |
| $\nu_{18}$ | 591 (4) | 584 (3) | 584 (4) | 579 (17) | 566 (16) | 573 (17) |
| $\nu_{19}$ | 547 (17) | 543 (20) | 542 (17) | 541 (10) | 532 (5) | 536 (10) |
| $\nu_{20}$ | 397 (4) | 393 (4) | 395 (4) | 387 (2) | 383 (2) | 385 (2) |
| $\nu_{21}$ | 223 (7) | 231 (4) | 226 (7) | 201 (6) | 205 (1) | 204 (6) |
| $\nu_{22}$ | 128 (3) | 162 (0) | 133 (3) | 179 (9) | 165 (13) | 182 (9) |
| $\nu_{23}$ | 103 (2) | 40 (3) | 108 (2) | 119 (0) | 76 (0) | 124 (0) |
| $\nu_{24}$ | 78 (28) | 80 (22) | 84 (28) | 56 (1) | 36 (1) | 62 (1) |

[a] Harmonic vibrational wavenumber scaled according to $0.9761\ x + 7.9$, in which $x$ is the harmonic vibrational wavenumber; this equation is only valid for wavenumbers below 2000 $cm^{-1}$.

**Table S6** Harmonic and anharmonic, and scaled harmonic vibrational wavenumbers ($cm^{-1}$) and IR intensities (km $mol^{-1}$, listed parenthetically) of conformers F3 and F4 of formic acetic anhydride (FAA) predicted with the B3LYP/aug-cc-pVTZ method

| Mode | F3 | | | F4 | | |
|---|---|---|---|---|---|---|
| | Harmonic | Anharmonic | Scaled harmonic[a] | Harmonic | Anharmonic | Scaled harmonic[a] |
| $\nu_1$ | 3153 (4) | 3014 (5) | | 3156 (3) | 3019 (3) | |
| $\nu_2$ | 3125 (3) | 2979 (2) | | 3106 (2) | 2972 (2) | |
| $\nu_3$ | 3060 (1) | 2949 (2) | | 3051 (15) | 3055 (3) | |
| $\nu_4$ | 3046 (42) | 2900 (41) | | 3041 (22) | 2791 (31) | |
| $\nu_5$ | 1869 (223) | 1836 (157) | 1832 (223) | 1871 (109) | 1852 (170) | 1834 (109) |
| $\nu_6$ | 1800 (365) | 1773 (338) | 1765 (365) | 1819 (579) | 1777 (356) | 1784 (579) |
| $\nu_7$ | 1478 (10) | 1428 (11) | 1450 (10) | 1489 (10) | 1443 (9) | 1461 (10) |
| $\nu_8$ | 1463 (15) | 1424 (16) | 1436 (15) | 1477 (11) | 1441 (7) | 1449 (11) |
| $\nu_9$ | 1405 (9) | 1380 (23) | 1380 (9) | 1414 (0) | 1385 (1) | 1388 (0) |
| $\nu_{10}$ | 1402 (28) | 1360 (14) | 1376 (28) | 1400 (34) | 1369 (32) | 1375 (34) |
| $\nu_{11}$ | 1166 (41) | 1136 (90) | 1146 (41) | 1202 (169) | 1174 (166) | 1181 (169) |
| $\nu_{12}$ | 1131 (584) | 1083 (410) | 1112 (584) | 1110 (440) | 1078 (341) | 1092 (440) |
| $\nu_{13}$ | 1072 (14) | 1052 (44) | 1054 (14) | 1066 (6) | 1043 (6) | 1048 (6) |
| $\nu_{14}$ | 1037 (3) | 1020 (4) | 1020 (3) | 1022 (0) | 1003 (0) | 1006 (0) |
| $\nu_{15}$ | 997 (168) | 961 (170) | 981 (168) | 996 (240) | 971 (261) | 980 (240) |
| $\nu_{16}$ | 790 (13) | 773 (13) | 779 (13) | 873 (5) | 858 (4) | 860 (5) |
| $\nu_{17}$ | 721 (60) | 697 (82) | 712 (60) | 626 (57) | 622 (36) | 619 (57) |
| $\nu_{18}$ | 590 (11) | 576 (11) | 583 (11) | 576 (4) | 574 (4) | 570 (4) |
| $\nu_{19}$ | 522 (4) | 516 (3) | 517 (4) | 512 (1) | 508 (1) | 508 (1) |
| $\nu_{20}$ | 417 (2) | 407 (2) | 415 (2) | 427 (8) | 432 (6) | 425 (8) |
| $\nu_{21}$ | 234 (10) | 227 (13) | 237 (10) | 244 (5) | 248 (2) | 246 (5) |
| $\nu_{22}$ | 219 (14) | 196 (19) | 222 (14) | 205 (1) | 201 (2) | 208 (1) |
| $\nu_{23}$ | 123 (0) | 65 (3) | 128 (0) | 121 (3) | 150 (0) | 126 (3) |
| $\nu_{24}$ | 39 (9) | 13 (3) | 46 (9) | 43 (13) | 34 (9) | 49 (13) |

[a] Harmonic vibrational wavenumber scaled according to $0.9761\,x + 7.9$, in which $x$ is the harmonic vibrational wavenumber; this equation is only valid for wavenumbers below 2000 $cm^{-1}$.

**Table S7** Rotational parameters of the ground state and vibrationally excited states ($v$ = 1) of conformers P1 and P2 of HPMA predicted with the B3LYP/aug-cc-pVTZ method

| Mode | HPMF (P1) | | | HPMF (P2) | | |
|---|---|---|---|---|---|---|
| | *A*'/*A*" | *B*'/*B*" | *C*'/*C*" | *A*'/*A*" | *B*'/*B*" | *C*'/*C*" |
| $\nu_7$ | 0.998 | 1.000 | 0.999 | 0.999 | 0.999 | 0.998 |
| $\nu_8$ | 1.001 | 0.998 | 0.999 | 1.002 | 1.000 | 1.000 |
| $\nu_9$ | 1.000 | 1.001 | 1.000 | 1.000 | 1.000 | 1.001 |
| $\nu_{10}$ | 1.000 | 1.001 | 1.000 | 1.001 | 1.002 | 1.003 |
| $\nu_{11}$ | 1.000 | 1.000 | 1.001 | 0.997 | 0.998 | 0.998 |
| $\nu_{12}$ | 0.999 | 0.998 | 0.999 | 0.998 | 0.999 | 0.998 |
| $\nu_{13}$ | 1.000 | 0.998 | 0.999 | 0.999 | 1.000 | 0.999 |
| $\nu_{14}$ | 0.998 | 1.001 | 1.001 | 0.999 | 1.000 | 0.999 |
| $\nu_{15}$ | 0.998 | 0.998 | 0.998 | 0.997 | 0.999 | 0.999 |
| $\nu_{16}$ | 1.002 | 0.999 | 0.999 | 1.001 | 0.999 | 1.000 |
| $\nu_{17}$ | 0.996 | 0.998 | 0.999 | 1.000 | 1.000 | 1.000 |
| $\nu_{18}$ | 1.000 | 1.000 | 1.000 | 0.995 | 1.000 | 1.002 |
| $\nu_{19}$ | 1.000 | 0.999 | 0.999 | 0.999 | 0.999 | 0.998 |
| $\nu_{20}$ | 0.999 | 0.997 | 0.998 | 1.000 | 0.996 | 0.996 |
| $\nu_{21}$ | 0.998 | 0.999 | 0.998 | 0.998 | 0.999 | 1.000 |
| $\nu_{22}$ | 0.999 | 0.999 | 0.998 | 0.996 | 1.000 | 1.002 |
| | *A*" / $cm^{-1}$ | *B*" / $cm^{-1}$ | *C*" / $cm^{-1}$ | *A*" / $cm^{-1}$ | *B*" / $cm^{-1}$ | *C*" / $cm^{-1}$ |
| $\nu = 0$ | 0.1853 | 0.0602 | 0.0484 | 0.1932 | 0.0493 | 0.0438 |

**Table S8** Rotational parameters of the ground state and vibrationally excited states ($v$ = 1) of conformers P3 and P4 of HPMA predicted with the B3LYP/aug-cc-pVTZ method

| Mode | HPMF (P3) | | | HPMF (P4) | | |
|---|---|---|---|---|---|---|
| | *A*'/*A*" | *B*'/*B*" | *C*'/*C*" | *A*'/*A*" | *B*'/*B*" | *C*'/*C*" |
| $\nu_7$ | 0.998 | 0.999 | 0.999 | 0.999 | 0.999 | 0.999 |
| $\nu_8$ | 1.000 | 0.999 | 1.001 | 1.001 | 1.000 | 0.999 |
| $\nu_9$ | 1.002 | 1.000 | 1.000 | 1.002 | 1.001 | 1.000 |
| $\nu_{10}$ | 1.000 | 1.000 | 1.001 | 1.001 | 0.999 | 1.000 |
| $\nu_{11}$ | 0.999 | 0.999 | 0.998 | 0.997 | 0.999 | 1.000 |
| $\nu_{12}$ | 0.998 | 1.000 | 0.999 | 0.996 | 1.000 | 0.999 |
| $\nu_{13}$ | 0.999 | 0.999 | 0.999 | 1.001 | 0.998 | 0.998 |
| $\nu_{14}$ | 0.999 | 1.000 | 1.000 | 0.997 | 1.002 | 1.002 |
| $\nu_{15}$ | 0.996 | 0.999 | 0.999 | 0.997 | 0.999 | 1.000 |
| $\nu_{16}$ | 1.003 | 0.999 | 0.998 | 1.000 | 0.999 | 0.999 |
| $\nu_{17}$ | 0.993 | 0.999 | 1.002 | 1.000 | 0.998 | 0.998 |
| $\nu_{18}$ | 1.000 | 1.000 | 1.000 | 0.999 | 0.999 | 0.999 |
| $\nu_{19}$ | 0.999 | 0.998 | 0.998 | 0.996 | 0.998 | 0.999 |
| $\nu_{20}$ | 0.999 | 0.998 | 0.998 | 0.996 | 1.000 | 0.999 |
| $\nu_{21}$ | 1.002 | 0.997 | 0.996 | 0.998 | 0.999 | 0.999 |
| $\nu_{22}$ | 0.998 | 0.998 | 0.999 | 0.997 | 0.999 | 1.000 |
| | *A*" / $cm^{-1}$ | *B*" / $cm^{-1}$ | *C*" / $cm^{-1}$ | *A*" / $cm^{-1}$ | *B*" / $cm^{-1}$ | *C*" / $cm^{-1}$ |
| $\nu = 0$ | 0.2110 | 0.0458 | 0.0402 | 0.1722 | 0.0524 | 0.0474 |

**Table S9** Rotational parameters of the ground state and vibrationally excited states ($v$ = 1) of conformer P5 of HPMA predicted with the B3LYP/aug-cc-pVTZ method

| Mode | HPMF (P5) | | |
|---|---|---|---|
| | *A*'/*A*" | *B*'/*B*" | *C*'/*C*" |
| $\nu_7$ | 0.999 | 0.998 | 0.998 |
| $\nu_8$ | 1.001 | 1.000 | 0.999 |
| $\nu_9$ | 1.001 | 1.000 | 1.000 |
| $\nu_{10}$ | 1.001 | 1.000 | 1.000 |
| $\nu_{11}$ | 0.998 | 0.998 | 1.001 |
| $\nu_{12}$ | 0.997 | 1.000 | 1.000 |
| $\nu_{13}$ | 0.999 | 1.000 | 1.000 |
| $\nu_{14}$ | 0.999 | 1.001 | 1.001 |
| $\nu_{15}$ | 0.997 | 1.000 | 1.000 |
| $\nu_{16}$ | 1.000 | 0.999 | 0.999 |
| $\nu_{17}$ | 1.000 | 0.997 | 0.996 |
| $\nu_{18}$ | 0.999 | 0.999 | 1.000 |
| $\nu_{19}$ | 0.996 | 0.999 | 1.001 |
| $\nu_{20}$ | 0.997 | 1.000 | 0.999 |
| $\nu_{21}$ | 0.997 | 1.000 | 0.999 |
| $\nu_{22}$ | 0.996 | 1.001 | 1.000 |
| | *A*" / $cm^{-1}$ | *B*" / $cm^{-1}$ | *C*" / $cm^{-1}$ |
| $\nu = 0$ | 0.1558 | 0.0553 | 0.0517 |

**Table S10** Rotational parameters of the ground state and vibrationally excited states ($v$ = 1) of conformers Q1 and Q2 of HSOZ predicted with the B3LYP/aug-cc-pVTZ method

| Mode | HSOZ (Q1) | | | HSOZ (Q2) | | |
|---|---|---|---|---|---|---|
| | *A*'/*A*" | *B*'/*B*" | *C*'/*C*" | *A*'/*A*" | *B*'/*B*" | *C*'/*C*" |
| $\nu_7$ | 1.000 | 1.000 | 1.001 | 1.000 | 1.000 | 1.001 |
| $\nu_8$ | 1.000 | 1.001 | 1.000 | 1.000 | 1.000 | 1.001 |
| $\nu_9$ | 1.001 | 1.000 | 1.001 | 1.000 | 1.001 | 1.000 |
| $\nu_{10}$ | 0.999 | 0.998 | 0.999 | 0.999 | 0.999 | 0.998 |
| $\nu_{11}$ | 1.000 | 1.000 | 0.998 | 1.000 | 0.999 | 0.999 |
| $\nu_{12}$ | 0.999 | 0.999 | 0.999 | 0.999 | 1.001 | 1.000 |
| $\nu_{13}$ | 1.001 | 1.000 | 1.001 | 1.000 | 0.999 | 1.000 |
| $\nu_{14}$ | 1.000 | 0.999 | 0.999 | 1.001 | 1.000 | 1.000 |
| $\nu_{15}$ | 0.999 | 1.000 | 0.999 | 0.997 | 0.996 | 0.999 |
| $\nu_{16}$ | 0.998 | 0.999 | 1.000 | 0.999 | 1.000 | 0.998 |
| $\nu_{17}$ | 0.999 | 0.998 | 0.998 | 0.998 | 0.999 | 0.999 |
| $\nu_{18}$ | 0.999 | 0.998 | 0.999 | 0.999 | 0.998 | 1.000 |
| $\nu_{19}$ | 0.998 | 1.000 | 0.999 | 0.998 | 1.000 | 0.998 |
| $\nu_{20}$ | 0.999 | 0.999 | 0.999 | 0.999 | 0.999 | 0.999 |
| $\nu_{21}$ | 1.000 | 1.000 | 0.999 | 1.000 | 1.000 | 0.999 |
| $\nu_{22}$ | 0.998 | 0.999 | 0.999 | 0.998 | 0.999 | 0.999 |
| $\nu_{23}$ | 0.999 | 0.998 | 0.998 | 0.999 | 0.997 | 0.998 |
| | *A*" / $cm^{-1}$ | *B*" / $cm^{-1}$ | *C*" / $cm^{-1}$ | *A*" / $cm^{-1}$ | *B*" / $cm^{-1}$ | *C*" / $cm^{-1}$ |
| $\nu = 0$ | 0.1537 | 0.0828 | 0.0796 | 0.1523 | 0.0835 | 0.0803 |

**Table S11** Rotational parameters of the ground state and vibrationally excited states ($v$ = 1) of conformers F1 and F2 of FAA predicted with the B3LYP/aug-cc-pVTZ method

| Mode | FAA (F1) | | | FAA (F2) | | |
|---|---|---|---|---|---|---|
| | *A*'/*A*" | *B*'/*B*" | *C*'/*C*" | *A*'/*A*" | *B*'/*B*" | *C*'/*C*" |
| $\nu_5$ | 0.982 | 0.998 | 0.998 | 0.997 | 0.999 | 0.999 |
| $\nu_6$ | 0.980 | 0.999 | 0.999 | 0.997 | 1.000 | 1.000 |
| $\nu_7$ | 0.986 | 1.001 | 1.000 | 1.001 | 1.001 | 1.000 |
| $\nu_8$ | 0.983 | 1.000 | 1.001 | 0.999 | 1.000 | 1.002 |
| $\nu_9$ | 0.980 | 0.999 | 0.998 | 0.998 | 1.000 | 1.000 |
| $\nu_{10}$ | 0.983 | 1.000 | 1.000 | 0.998 | 0.999 | 1.000 |
| $\nu_{11}$ | 0.980 | 0.998 | 0.997 | 0.998 | 0.999 | 0.998 |
| $\nu_{12}$ | 0.983 | 0.999 | 1.000 | 1.004 | 0.997 | 0.996 |
| $\nu_{13}$ | 0.984 | 0.997 | 0.998 | 1.001 | 0.999 | 0.999 |
| $\nu_{14}$ | 0.983 | 0.999 | 1.000 | 1.000 | 0.998 | 0.999 |
| $\nu_{15}$ | 0.980 | 0.999 | 0.999 | 0.995 | 0.999 | 1.001 |
| $\nu_{16}$ | 0.982 | 0.997 | 0.997 | 0.999 | 0.997 | 0.999 |
| | *A*" / $cm^{-1}$ | *B*" / $cm^{-1}$ | *C*" / $cm^{-1}$ | *A*" / $cm^{-1}$ | *B*" / $cm^{-1}$ | *C*" / $cm^{-1}$ |
| $\nu = 0$ | 0.3240 | 0.0741 | 0.0610 | 0.2668 | 0.0879 | 0.0728 |

**Table S12** Rotational parameters of the ground state and vibrationally excited states ($v$ = 1) of conformers F3 and F4 of FAA predicted with the B3LYP/aug-cc-pVTZ method

| Mode | FAA (F3) | | | FAA (F4) | | |
|---|---|---|---|---|---|---|
| | *A*'/*A*" | *B*'/*B*" | *C*'/*C*" | *A*'/*A*" | *B*'/*B*" | *C*'/*C*" |
| $\nu_5$ | 1.005 | 0.998 | 0.994 | 0.999 | 0.999 | 0.999 |
| $\nu_6$ | 0.995 | 0.999 | 1.002 | 1.001 | 1.000 | 1.000 |
| $\nu_7$ | 1.002 | 0.999 | 1.001 | 1.006 | 1.001 | 1.001 |
| $\nu_8$ | 1.007 | 1.000 | 0.997 | 0.996 | 1.000 | 1.001 |
| $\nu_9$ | 0.996 | 1.001 | 1.002 | 0.999 | 1.000 | 0.998 |
| $\nu_{10}$ | 0.992 | 1.000 | 1.001 | 0.996 | 1.000 | 0.999 |
| $\nu_{11}$ | 1.000 | 0.999 | 0.998 | 1.003 | 0.998 | 0.999 |
| $\nu_{12}$ | 0.997 | 0.998 | 0.998 | 1.003 | 0.999 | 0.999 |
| $\nu_{13}$ | 1.000 | 1.000 | 0.999 | 0.998 | 1.002 | 1.003 |
| $\nu_{14}$ | 0.997 | 0.999 | 1.001 | 1.000 | 1.000 | 1.000 |
| $\nu_{15}$ | 0.993 | 0.999 | 1.001 | 0.998 | 0.998 | 0.997 |
| $\nu_{16}$ | 0.997 | 0.998 | 1.001 | 1.000 | 1.001 | 1.001 |
| | *A*" / $cm^{-1}$ | *B*" / $cm^{-1}$ | *C*" / $cm^{-1}$ | *A*" / $cm^{-1}$ | *B*" / $cm^{-1}$ | *C*" / $cm^{-1}$ |
| $\nu = 0$ | 0.2324 | 0.0944 | 0.0753 | 0.2991 | 0.0751 | 0.0608 |

**Table S13** Ratios of *a*-, *b*-, and *c*-types of vibrational bands for each vibrational mode of conformers P1 and P2 of HPMA predicted with the B3LYP/aug-cc-pVTZ method

| Mode | HPMF (P1) | | | HPMF (P2) | | |
|---|---|---|---|---|---|---|
| | *a*-type | *b*-type | *c*-type | *a*-type | *b*-type | *c*-type |
| $\nu_7$ | 0.03 | 0.06 | 0.01 | 0.02 | 0.06 | 0.02 |
| $\nu_8$ | 0.07 | 0.07 | 0.02 | 0.12 | 0.12 | 0.29 |
| $\nu_9$ | 0.05 | 0.04 | 0.34 | 0.03 | 0.24 | 0.09 |
| $\nu_{10}$ | 0.21 | 0.01 | 0.16 | 0.21 | 0.12 | 0.13 |
| $\nu_{11}$ | 0.08 | 0.18 | 0.02 | 0.05 | 0.19 | 0.12 |
| $\nu_{12}$ | 0.14 | 0.09 | 0.03 | 0.17 | 0.08 | 0.01 |
| $\nu_{13}$ | 0.21 | 0.00 | 0.02 | 0.09 | 0.11 | 0.01 |
| $\nu_{14}$ | 0.22 | 0.41 | 0.05 | 0.69 | 0.16 | 0.66 |
| $\nu_{15}$ | 0.05 | 0.04 | 0.00 | 0.05 | 0.00 | 0.02 |
| $\nu_{16}$ | 0.18 | 0.05 | 0.10 | 0.21 | 0.11 | 0.15 |
| $\nu_{17}$ | 0.09 | 0.08 | 0.08 | 0.22 | 0.06 | 0.24 |
| $\nu_{18}$ | 0.02 | 0.03 | 0.40 | 0.08 | 0.05 | 0.17 |
| $\nu_{19}$ | 0.09 | 0.03 | 0.01 | 0.07 | 0.01 | 0.00 |
| $\nu_{20}$ | 0.10 | 0.03 | 0.01 | 0.08 | 0.02 | 0.00 |
| $\nu_{21}$ | 0.12 | 0.02 | 0.02 | 0.15 | 0.06 | 0.06 |
| $\nu_{22}$ | 0.19 | 0.06 | 0.00 | 0.03 | 0.21 | 0.13 |

**Table S14** Ratios of *a*-, *b*-, and *c*-types of vibrational bands for each vibrational mode of conformers P3 and P4 of HPMA predicted with the B3LYP/aug-cc-pVTZ method

| Mode | HPMF (P3) | | | HPMF (P4) | | |
|---|---|---|---|---|---|---|
| | *a*-type | *b*-type | *c*-type | *a*-type | *b*-type | *c*-type |
| $\nu_7$ | 0.02 | 0.05 | 0.01 | 0.04 | 0.04 | 0.01 |
| $\nu_8$ | 0.12 | 0.32 | 0.15 | 0.09 | 0.05 | 0.36 |
| $\nu_9$ | 0.07 | 0.11 | 0.33 | 0.06 | 0.07 | 0.35 |
| $\nu_{10}$ | 0.07 | 0.24 | 0.06 | 0.21 | 0.07 | 0.10 |
| $\nu_{11}$ | 0.04 | 0.22 | 0.06 | 0.14 | 0.02 | 0.30 |
| $\nu_{12}$ | 0.15 | 0.03 | 0.01 | 0.10 | 0.12 | 0.06 |
| $\nu_{13}$ | 0.07 | 0.10 | 0.09 | 0.09 | 0.09 | 0.03 |
| $\nu_{14}$ | 0.39 | 0.03 | 0.09 | 0.23 | 0.05 | 0.01 |
| $\nu_{15}$ | 0.05 | 0.00 | 0.00 | 0.05 | 0.02 | 0.03 |
| $\nu_{16}$ | 0.13 | 0.01 | 0.08 | 0.20 | 0.03 | 0.01 |
| $\nu_{17}$ | 0.18 | 0.09 | 0.05 | 0.09 | 0.05 | 0.00 |
| $\nu_{18}$ | 0.04 | 0.10 | 0.41 | 0.09 | 0.07 | 0.06 |
| $\nu_{19}$ | 0.07 | 0.01 | 0.01 | 0.09 | 0.04 | 0.05 |
| $\nu_{20}$ | 0.13 | 0.02 | 0.00 | 0.08 | 0.00 | 0.00 |
| $\nu_{21}$ | 0.08 | 0.13 | 0.03 | 0.16 | 0.00 | 0.11 |
| $\nu_{22}$ | 0.21 | 0.03 | 0.01 | 0.17 | 0.20 | 0.16 |

**Table S15** Ratios of *a*-, *b*-, and *c*-types of vibrational bands for each vibrational mode of conformer P5 predicted with the B3LYP/aug-cc-pVTZ method

| Mode | HPMF (P5) | | |
|---|---|---|---|
| | *a*-type | *b*-type | *c*-type |
| $\nu_7$ | 0.04 | 0.02 | 0.03 |
| $\nu_8$ | 0.71 | 0.34 | 0.67 |
| $\nu_9$ | 0.15 | 0.18 | 0.18 |
| $\nu_{10}$ | 0.22 | 0.02 | 0.18 |
| $\nu_{11}$ | 0.07 | 0.21 | 0.10 |
| $\nu_{12}$ | 0.08 | 0.13 | 0.03 |
| $\nu_{13}$ | 0.01 | 0.13 | 0.11 |
| $\nu_{14}$ | 0.21 | 0.01 | 0.01 |
| $\nu_{15}$ | 0.05 | 0.03 | 0.00 |
| $\nu_{16}$ | 0.04 | 0.39 | 1.08 |
| $\nu_{17}$ | 0.08 | 0.02 | 0.03 |
| $\nu_{18}$ | 0.10 | 0.01 | 0.17 |
| $\nu_{19}$ | 0.10 | 0.01 | 0.00 |
| $\nu_{20}$ | 0.08 | 0.03 | 0.01 |
| $\nu_{21}$ | 0.15 | 0.04 | 0.08 |
| $\nu_{22}$ | 0.13 | 0.30 | 0.21 |

**Table S16** Ratios of *a*-, *b*-, and *c*-types of vibrational bands for each vibrational mode of conformers Q1 and Q2 of HSOZ predicted with the B3LYP/aug-cc-pVTZ method

| Mode | HSOZ (Q1) | | | HSOZ (Q2) | | |
|---|---|---|---|---|---|---|
| | *a*-type | *b*-type | *c*-type | *a*-type | *b*-type | *c*-type |
| $\nu_7$ | 0.13 | 0.89 | 0.47 | 1.02 | 1.19 | 1.02 |
| $\nu_8$ | 0.53 | 0.28 | 0.82 | 0.04 | 0.63 | 0.25 |
| $\nu_9$ | 0.12 | 0.32 | 0.51 | 0.04 | 0.31 | 0.59 |
| $\nu_{10}$ | 0.13 | 0.01 | 0.01 | 0.12 | 0.05 | 0.11 |
| $\nu_{11}$ | 0.13 | 0.19 | 0.12 | 0.03 | 0.21 | 0.19 |
| $\nu_{12}$ | 0.14 | 0.07 | 0.05 | 0.07 | 0.05 | 0.09 |
| $\nu_{13}$ | 0.08 | 0.26 | 0.18 | 0.12 | 0.13 | 0.01 |
| $\nu_{14}$ | 0.03 | 0.05 | 0.03 | 0.02 | 0.12 | 0.07 |
| $\nu_{15}$ | 0.05 | 0.12 | 0.25 | 0.05 | 0.02 | 0.04 |
| $\nu_{16}$ | 0.09 | 0.05 | 0.09 | 0.26 | 0.04 | 0.04 |
| $\nu_{17}$ | 0.09 | 0.04 | 0.06 | 0.04 | 0.09 | 0.01 |
| $\nu_{18}$ | 0.06 | 0.06 | 0.01 | 0.09 | 0.04 | 0.00 |
| $\nu_{19}$ | 0.09 | 0.03 | 0.09 | 0.11 | 0.03 | 0.08 |
| $\nu_{20}$ | 0.07 | 0.09 | 0.02 | 0.04 | 0.10 | 0.03 |
| $\nu_{21}$ | 0.17 | 0.12 | 0.25 | 0.40 | 0.48 | 0.32 |
| $\nu_{22}$ | 0.06 | 0.10 | 0.14 | 0.02 | 0.12 | 0.15 |
| $\nu_{23}$ | 0.21 | 0.16 | 0.01 | 0.51 | 0.01 | 0.35 |

**Table S17** Ratios of *a*-, *b*-, and *c*-types of vibrational bands for each vibrational mode of conformers F1 and F2 of FAA predicted with the B3LYP/aug-cc-pVTZ method

| Mode | FAA (F1) | | | FAA (F2) | | |
|---|---|---|---|---|---|---|
| | *a*-type | *b*-type | *c*-type | *a*-type | *b*-type | *c*-type |
| $\nu_5$ | 0.07 | 0.02 | 0.00 | 0.02 | 0.05 | 0.00 |
| $\nu_6$ | 0.03 | 0.04 | 0.00 | 0.06 | 0.01 | 0.05 |
| $\nu_7$ | 0.00 | 0.00 | 0.34 | 0.10 | 0.00 | 0.32 |
| $\nu_8$ | 0.05 | 0.25 | 0.00 | 0.00 | 0.26 | 0.01 |
| $\nu_9$ | 0.13 | 0.05 | 0.00 | 0.20 | 0.07 | 0.03 |
| $\nu_{10}$ | 0.84 | 0.02 | 0.00 | 0.22 | 0.06 | 0.10 |
| $\nu_{11}$ | 0.06 | 0.01 | 0.00 | 0.08 | 0.03 | 0.01 |
| $\nu_{12}$ | 0.00 | 0.00 | 0.38 | 0.04 | 0.01 | 0.00 |
| $\nu_{13}$ | 0.04 | 0.01 | 0.00 | 0.08 | 0.02 | 0.01 |
| $\nu_{14}$ | 0.00 | 0.00 | 3.51 | 0.15 | 0.03 | 0.00 |
| $\nu_{15}$ | 0.11 | 0.30 | 0.00 | 0.09 | 0.01 | 0.01 |
| $\nu_{16}$ | 0.09 | 0.04 | 0.00 | 0.09 | 0.14 | 0.05 |

**Table S18** Ratios of *a*-, *b*-, and *c*-types of vibrational bands for each vibrational mode of conformers F3 and F4 of FAA predicted with the B3LYP/aug-cc-pVTZ method

| Mode | FAA (F3) | | | FAA (F4) | | |
|---|---|---|---|---|---|---|
| | *a*-type | *b*-type | *c*-type | *a*-type | *b*-type | *c*-type |
| $\nu_5$ | 0.05 | 0.03 | 0.03 | 0.01 | 0.10 | 0.00 |
| $\nu_6$ | 0.03 | 0.04 | 0.02 | 0.04 | 0.01 | 0.00 |
| $\nu_7$ | 0.19 | 0.08 | 0.23 | 0.00 | 0.00 | 0.31 |
| $\nu_8$ | 0.21 | 0.01 | 0.16 | 0.26 | 0.14 | 0.00 |
| $\nu_9$ | 0.29 | 0.17 | 0.04 | 0.40 | 1.95 | 0.00 |
| $\nu_{10}$ | 0.02 | 0.19 | 0.02 | 0.10 | 0.14 | 0.00 |
| $\nu_{11}$ | 0.01 | 0.16 | 0.00 | 0.06 | 0.04 | 0.00 |
| $\nu_{12}$ | 0.04 | 0.00 | 0.00 | 0.05 | 0.02 | 0.00 |
| $\nu_{13}$ | 0.20 | 0.04 | 0.17 | 0.00 | 0.00 | 0.41 |
| $\nu_{14}$ | 0.47 | 0.27 | 0.12 | 0.00 | 0.00 | 5.13 |
| $\nu_{15}$ | 0.07 | 0.03 | 0.00 | 0.07 | 0.00 | 0.00 |
| $\nu_{16}$ | 0.15 | 0.21 | 0.09 | 0.03 | 0.45 | 0.00 |

**Table S19** Experimental conditions and fitted $[CH_2OO]_0$ in varied sets of experiments of $CH_2I + O_2$

| Set | Expt. | $[CH_2I_2]_0$ /$10^{15}$ [a] | $[O_2]_0$ /$10^{17}$ [a] | $[CH_2OO]_0$ /$10^{14}$ [a] |
|---|---|---|---|---|
| 1 | 1 | 4.6 | 9.7 | 2.19 |
| | 2 | 3.8 | 9.7 | 2.16 |
| | 3 | 3.0 | 9.7 | 1.67 |
| | 4 | 2.1 | 9.7 | 1.33 |
| 2 | 5 | 4.5 | 13.0 | 2.24 |
| | 6 | 3.9 | 13.0 | 2.0 |
| | 7 | 3.2 | 13.0 | 1.84 |
| | 8 | 2.4 | 13.0 | 1.40 |

[a] in unit of molecule $cm^{-3}$

**Table S20** Kinetic model employed in fitting the temporal profiles of $CH_2OO$ and HPMA

| | Reaction | Rate coefficient [a] | Ref. |
|---|---|---|---|
| $k_1$* | $CH_2I + O_2 \rightarrow CH_2OO + I$ | $1.2\times10^{-12}$ | 3 |
| $k_2$* | $CH_2I + O_2 \rightarrow ICH_2OO$ | $1.9\times10^{-13}$ | 3 |
| $k_3$* | $CH_2I + O_2 \rightarrow$ other + I | $1.2\times10^{-13}$ | 3 |
| $k_4$* | $CH_2I + O_2 \rightarrow H_2CO + IO$ | $4.0\times10^{-13}$ | 8 |
| $k_5$* | $CH_2OO + I \rightarrow CH_2I + O_2$ | 55 $k_1$* | 3 |
| $k_6$* | $CH_2OO + I \rightarrow ICH_2OO$ | 55 $k_2$* | 3 |
| $k_7$* | $CH_2OO + I \rightarrow H_2CO + IO$ | $9.0\times10^{-12}$ | 3 |
| $k_8$* | $CH_2OO + CH_2I \rightarrow C_2H_4I + O_2$ | $6.3\times10^{-11}$ | 4 |
| $k_9$* | $2CH_2OO \rightarrow 2H_2CO + O_2$ | $8.0\times10^{-11}$ | 3-4 |
| $k_{10}$* | $ICH_2OO + I \rightarrow ICH_2O + IO$ | $3.5\times10^{-11}$ | 9 |
| $k_{11}$* | $2ICH_2OO \rightarrow 2ICH_2O + O_2$ | $9.0\times10^{-11}$ | 9 |
| $k_{12}$* | $ICH_2O \rightarrow H_2CO + I$ | $10^6$ $s^{-1}$ | 9 |
| $k_{13}$* | $2IO \rightarrow I_2 + O_2$ | $9.9\times10^{-11}$ | 10 |
| $k_{14}$* | $CH_2OO + CH_3C(O)OH \rightarrow$ HPMA | $k^I = k_{14}$*×$[CH_3C(O)OH]_0$, fitted | |

[a] rate coefficient in $cm^3$ $molecule^{-1}$ $s^{-1}$, unless specified otherwise.

**Table S21** Experimental conditions and first-order rate coefficients $k^{I}$ of reaction $CH_2OO$ + $CH_3C(O)OH$ in varied sets of experiments

| Set | Expt. | $[CH_2I_2]_0$ /$10^{14}$ [a] | $[CH_3C(O)OH]_0$ /$10^{15}$ [a] | $[O_2]_0$ /$10^{18}$ [a] | $[CH_2I]_0$ /$10^{14}$ [a] | $k^{I}$ /$10^{5}$ $s^{-1}$ |
|---|---|---|---|---|---|---|
| 1 | 1 | 9.8 | 0.61 | 1.3 | 2.4 | 0.53 |
| | 2 | 9.6 | 1.24 | 1.3 | 2.1 | 1.5 |
| | 3 | 9.7 | 1.88 | 1.3 | 2.0 | 2.3 |
| | 4 | 10.1 | 2.37 | 1.3 | 2.1 | 2.88 |
| | 5 | 10.1 | 3.03 | 1.3 | 1.9 | 3.86 |
| | 6 | 10.1 | 3.57 | 1.3 | 1.9 | 4.45 |
| 2 | 7 | 8.3 | 0.89 | 1.3 | 1.9 | 1.03 |
| | 8 | 8.3 | 1.42 | 1.3 | 1.8 | 1.79 |
| | 9 | 8.3 | 1.93 | 1.3 | 1.7 | 2.48 |
| | 10 | 8.2 | 2.31 | 1.3 | 1.6 | 3.05 |
| | 11 | 8.2 | 2.64 | 1.3 | 1.6 | 3.16 |
| | 12 | 8.4 | 3.2 | 1.3 | 1.5 | 3.92 |
| | 13 | 8.4 | 3.56 | 1.3 | 1.4 | 4.83 |
| 3 | 14 | 13.1 | 0.51 | 1.3 | 3.5 | 0.5 |
| | 15 | 13.0 | 0.83 | 1.3 | 3.4 | 0.96 |
| | 16 | 13.3 | 1.27 | 1.3 | 3.2 | 1.43 |
| | 17 | 13.3 | 1.8 | 1.3 | 3.1 | 2.03 |
| | 18 | 13.3 | 2.15 | 1.3 | 3.1 | 2.46 |
| | 19 | 13.3 | 2.66 | 1.3 | 3.0 | 3.15 |
| | 20 | 13.3 | 3.05 | 1.3 | 3.0 | 3.76 |
| 4 | 21 | 13.2 | 0.53 | 2.6 | 2.4 | 0.62 |
| | 22 | 13.2 | 0.86 | 2.6 | 2.4 | 1.13 |
| | 23 | 13.0 | 1.32 | 2.6 | 2.3 | 1.89 |
| | 24 | 13.1 | 1.88 | 2.6 | 2.2 | 2.59 |
| | 25 | 13.1 | 2.26 | 2.6 | 2.3 | 3.17 |
| | 26 | 13.1 | 2.84 | 2.6 | 2.3 | 3.78 |
| | 27 | 13.1 | 3.26 | 2.6 | 2.3 | 4.45 |
| 5 | 28 | 13.1 | 1.14 | 3.3 | 2.3 | 1.75 |
| | 29 | 13.3 | 1.68 | 3.3 | 2.4 | 2.23 |
| | 30 | 13.3 | 2.08 | 3.3 | 2.1 | 3.04 |
| | 31 | 13.3 | 3.0 | 3.3 | 2.1 | 4.12 |

[a] in unit of molecule $cm^{-3}$

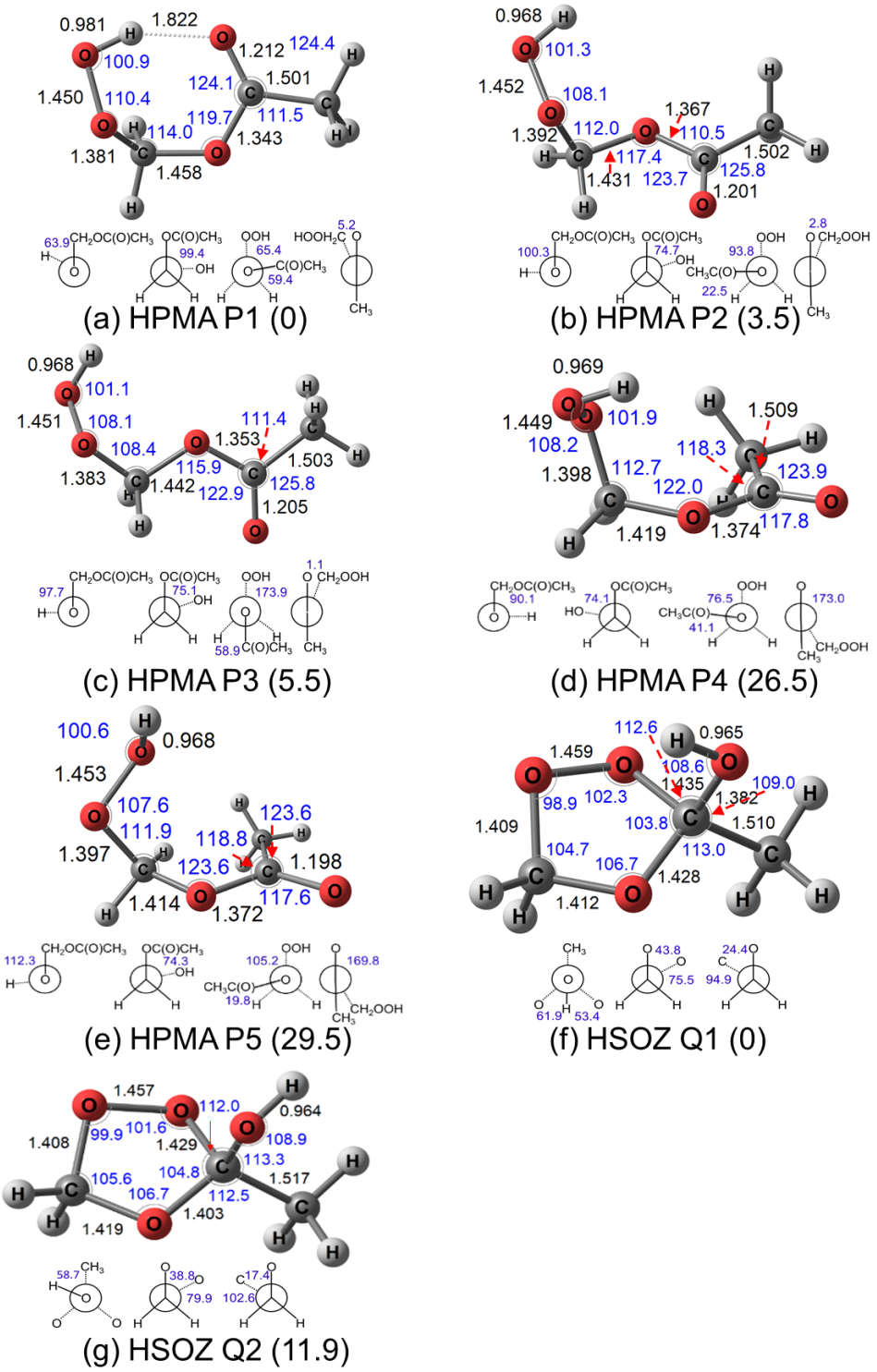


**Fig. S1** Geometries of possible intermediates in reaction $CH_2OO$ + $CH_3C(O)OH$. The conformations are indicated. Conformers of hydroperoxymethyl acetate (HPMA): (a) P1, (b) P2, (c) P3, (d) P4, (e) P5. Conformers of hydroxylated secondary ozonide (HSOZ): (f) Q1 and (g) Q2. Relative energies with respect to the least-energy conformer is presented in parentheses. The structures are calculated with the B3LYP/aug-cc-pVTZ method and the energies are calculated with the CCSD(T)/aug-cc-pVTZ//B3LYP/aug-cc-PVTZ method. Bond distances (black) are in Å and bond angles (in blue) are in degree.

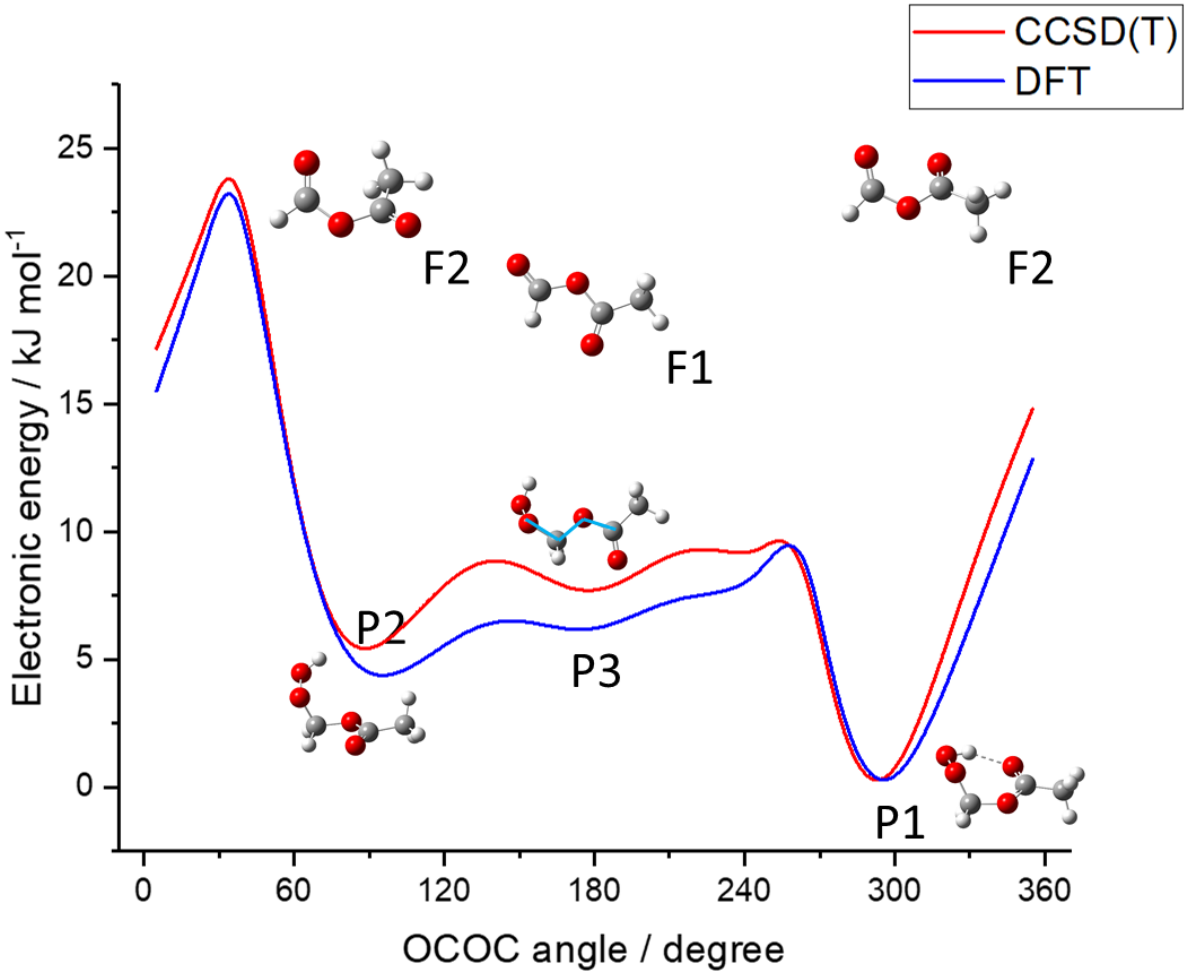


**Fig. S2** Potential energy curve calculated as a function of the OCOC dihedral angle of HPMA P1−P3. The bonds involved in the dihedral angle is schematically given in light blue lines in the structure of the P3 conformer. Blue and red lines signifies the energies calculated with the B3LYP/aug-cc-pVTZ and CCSD(T)/aug-cc-pVTZ//B3LYP/aug-cc-pVTZ methods. The zero of energy is set as that of the most stable conformer P1. Possible unimolecular dehydration reaction products, FAA, are also given above each HPMA conformation for comparison.

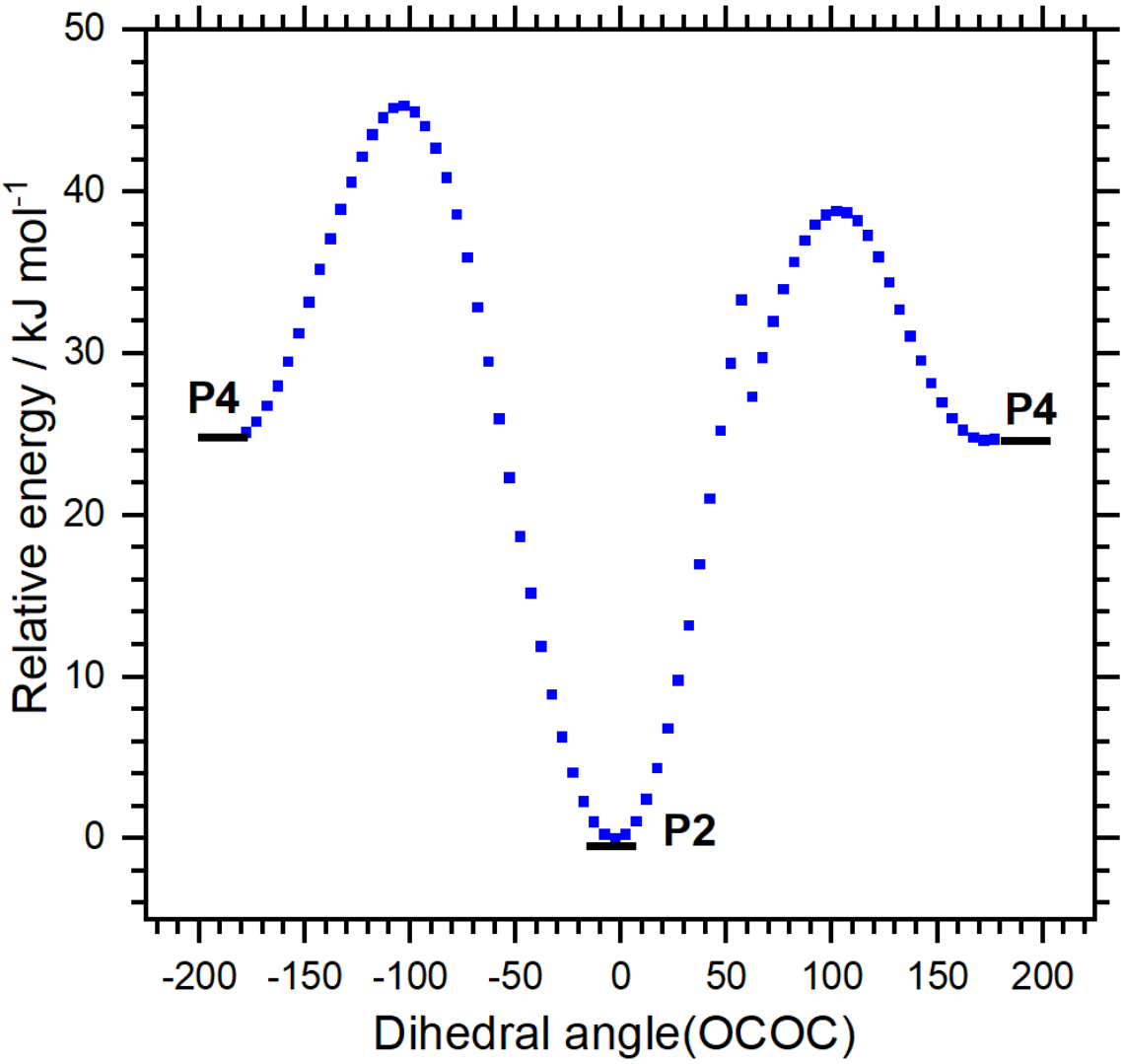


**Fig. S3** Potential energy of relaxed scans for the interconversion between conformers P2 and P4 calculated with the B3LYP/aug-cc-pVTZ method.

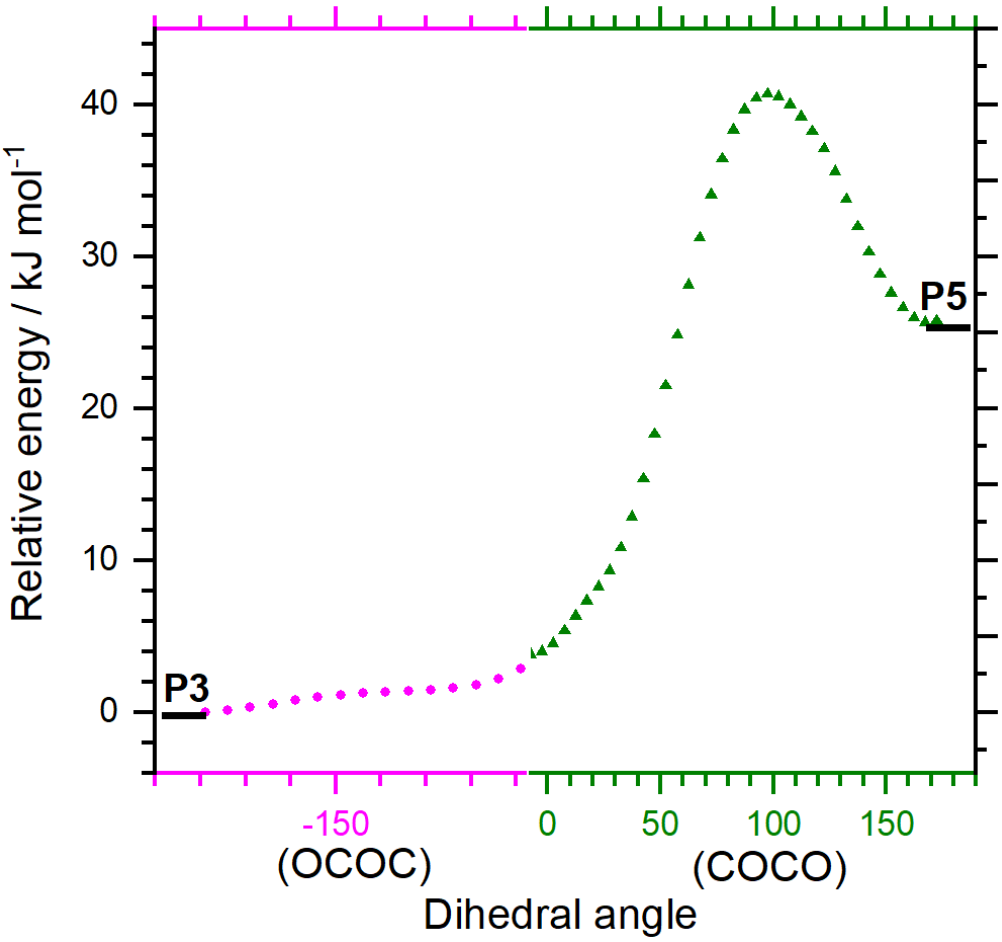


**Fig. S4** Potential energy of relaxed scans for the interconversion of conformers P3 and P5 calculated with the B3LYP/aug-cc-pVTZ method. We connected two scans to present the interconversion in the same figure.

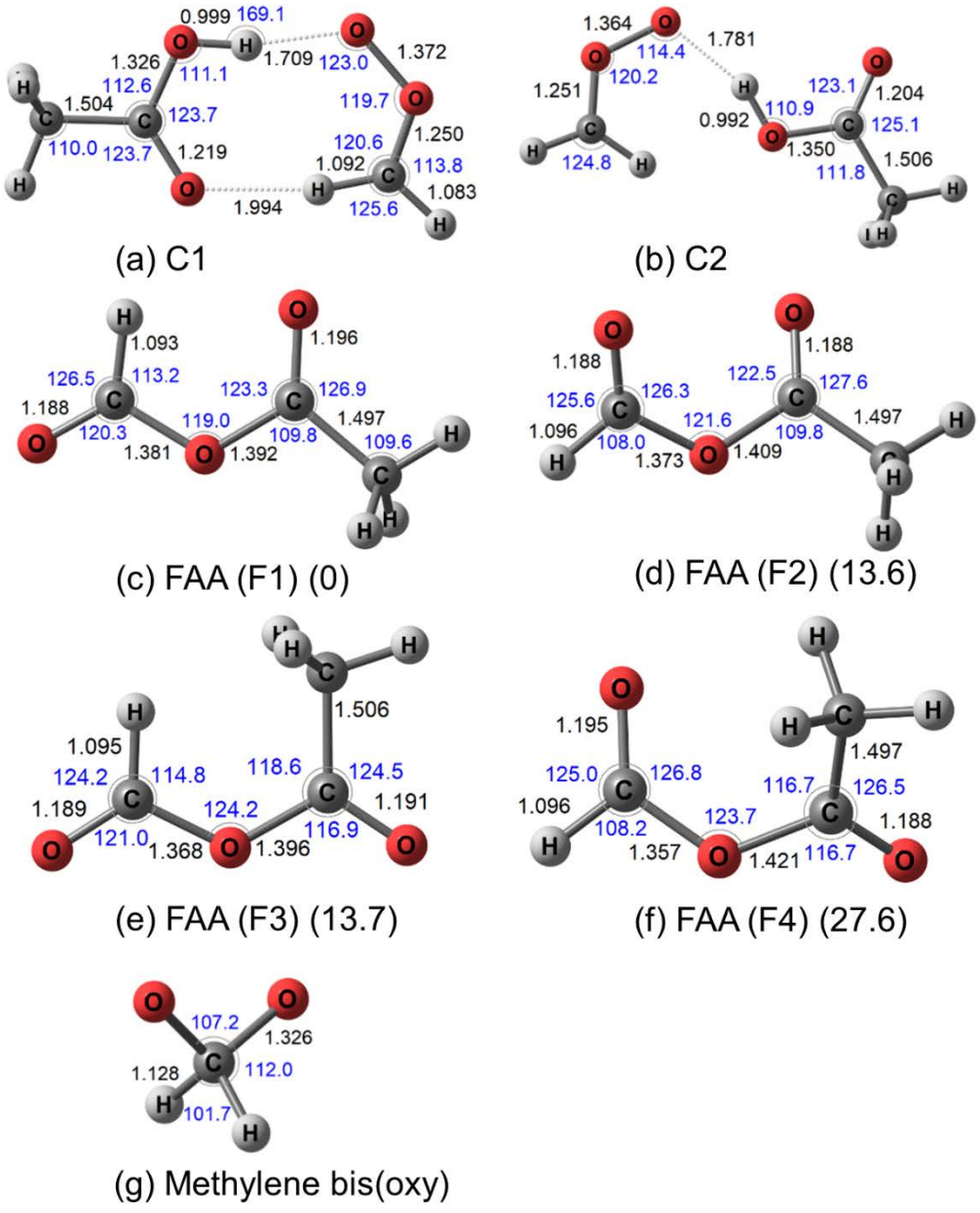


**Fig. S5** Geometries of pre-reactive complexes and products in reaction $CH_2OO + CH_3C(O)OH$. The conformation of FAA are denoted in parentheses. Conformers of complexes: (a) C1 and (b) C2. Conformers of formic acetic anhydride FAA: (c) F1, (d) F2, (e) F3, (f) F4, and (g) methylene bis(oxy). Relative energies with respect to the least-energy conformer is presented in parentheses. The structures are calculated with the B3LYP/aug-cc-pVTZ method and the energies are calculated with the CCSD(T)/aug-cc-pVTZ//B3LYP/aug-cc-PVTZ method. Bond distances (black) are in Å and bond angles (in blue) are in degree.

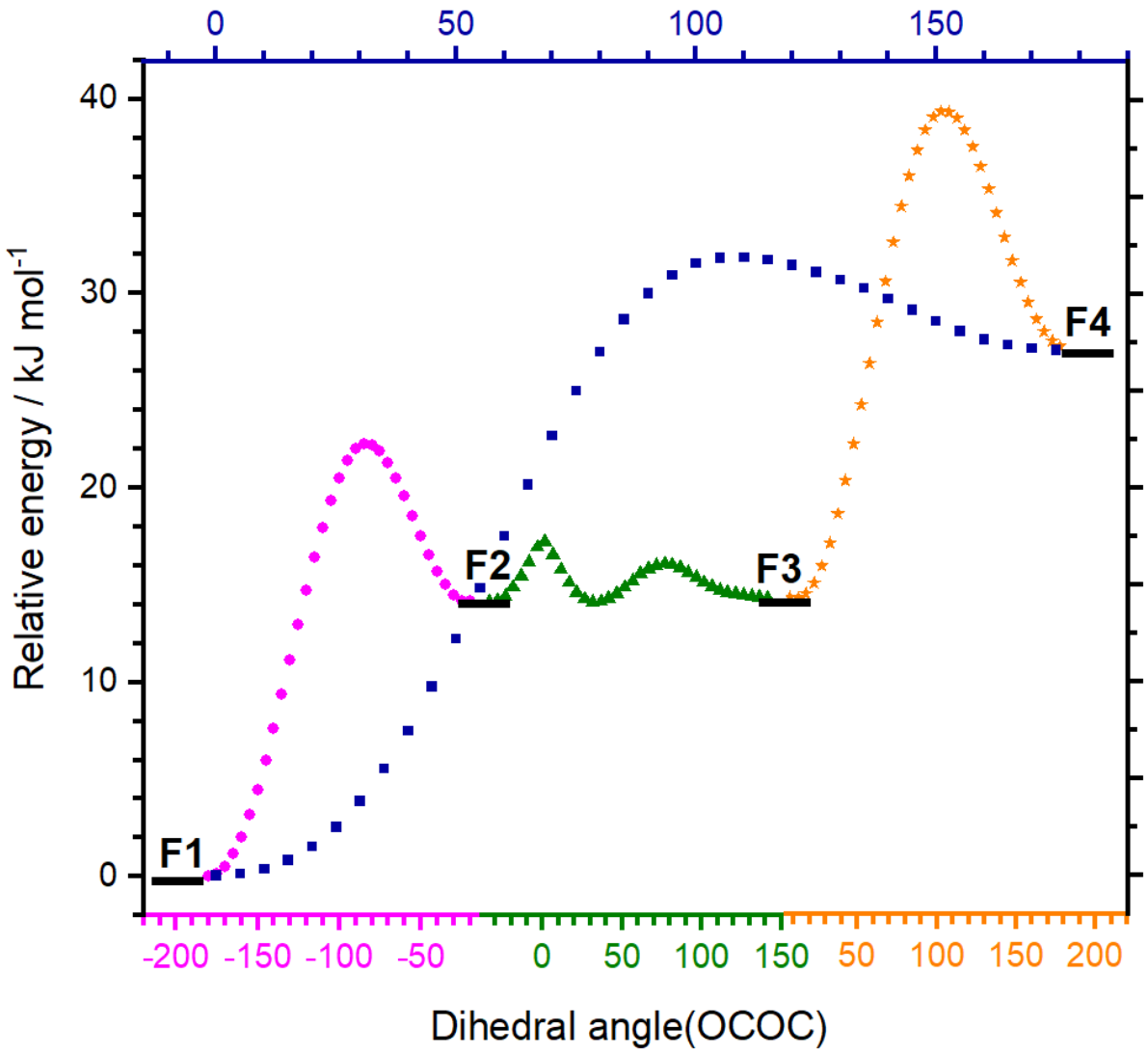


**Fig. S6** Potential energy of relaxed scans for the interconversion among conformers of formic acetic anhydride (FAA) calculated with the B3LYP/aug-cc-pVTZ method. We connected multiple scans to present the interconversion in the same figure. The scan for F1− F2, F2−F3, F3−F4, and F1-F4 are presented in pink, green, orange, and blue colors, respectively. The bottom x-axis represents the dihedral angle for the F1− F2, F2−F3, and F3−F4 scans. The top x-axis represents the dihedral angle for the F1− F4 scan.

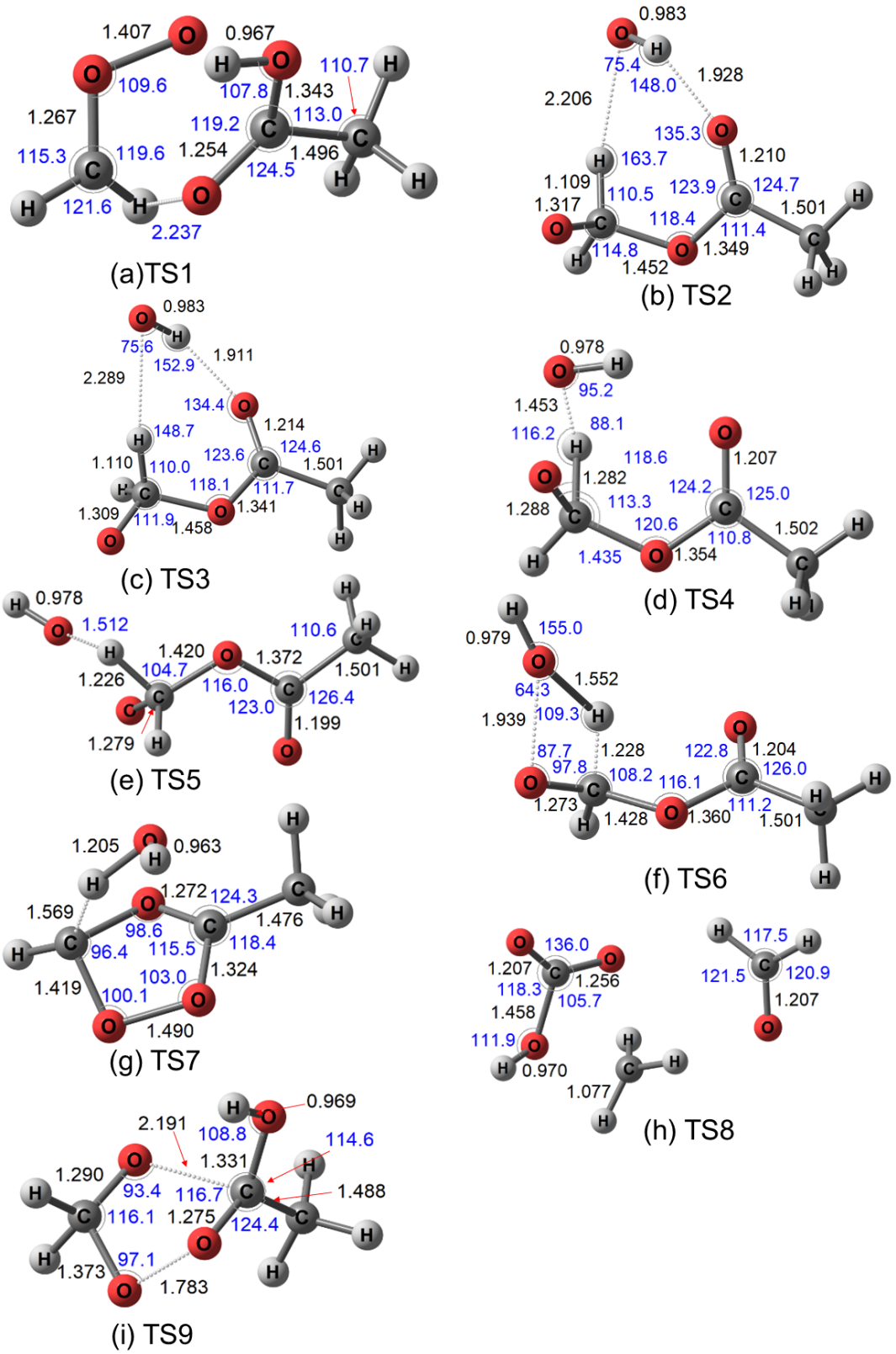


**Fig. S7** Geometries of the transition states in reaction $CH_2OO$ + $CH_3C(O)OH$. (a) TS1, (b) TS2, (c) TS3, (d) TS4, (e) TS5, (f) TS6, (g) TS7, (h) TS8, and (i) TS9. Bond distances (black) are in Å and bond angles (in blue) are in degree.

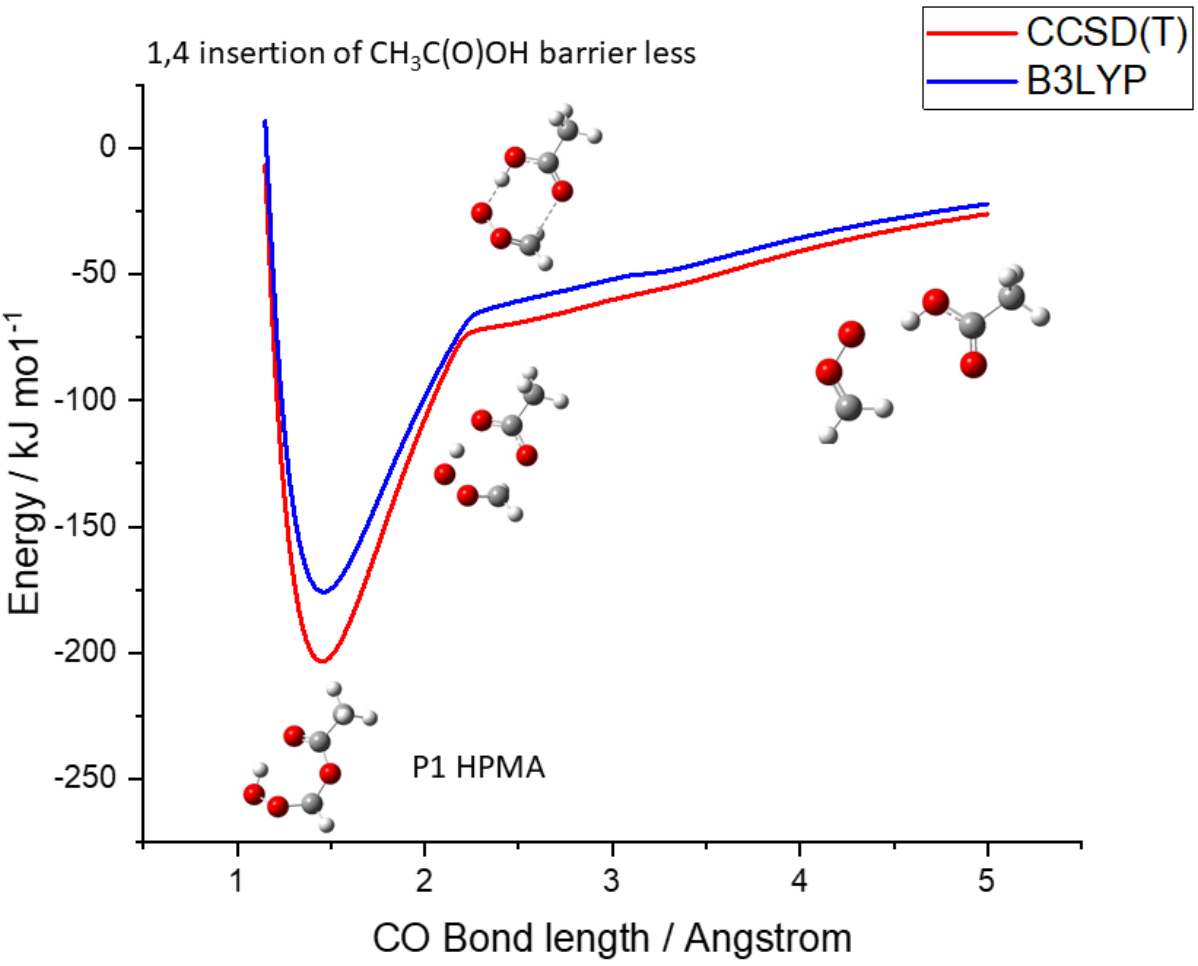


**Fig. S8** Potential energy curve calculated as a function of the distance between the carbon atom of $CH_2OO$ and the carbonyl oxygen atom of $CH_3C(O)OH$. Blue and red lines signifies the energies calculated with the B3LYP/aug-cc-pVTZ and CCSD(T)/aug-cc-pVTZ//B3LYP/aug-cc-pVTZ method. The zero of energy is set as that of infinitely separated $CH_2OO$ and $CH_3C(O)OH$.

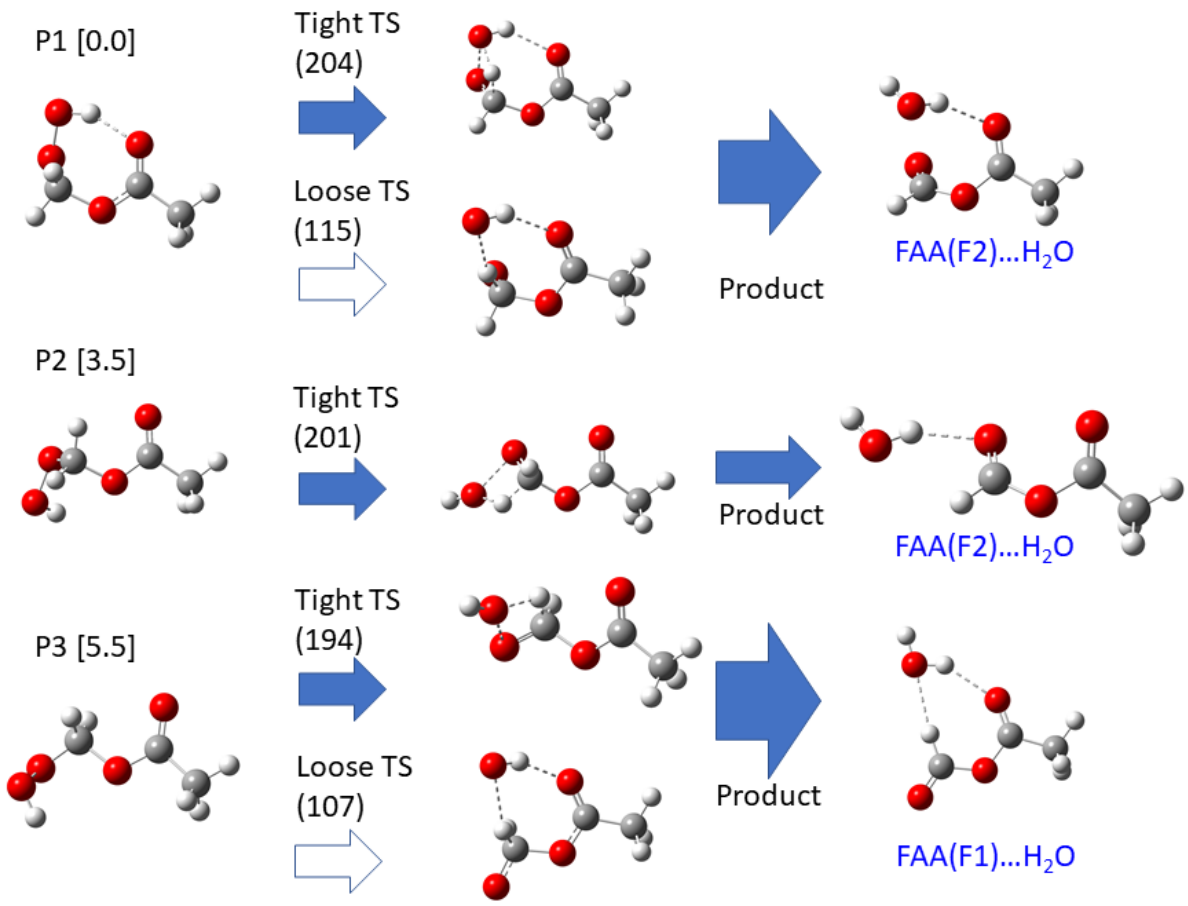


**Fig. S9** Schematic geometries of different HPMA conformations and their possible dehydration reaction transition states (TS). For P1 and P3, we list both the tight and loose TS. The values in square brackets are the zero-point corrected energy difference between each HPMA conformers in kJ $mol^{-1}$. The values in parenthesis are the zero-point corrected energy difference between each HPMA conformer and its respective TS in kJ $mol^{-1}$.

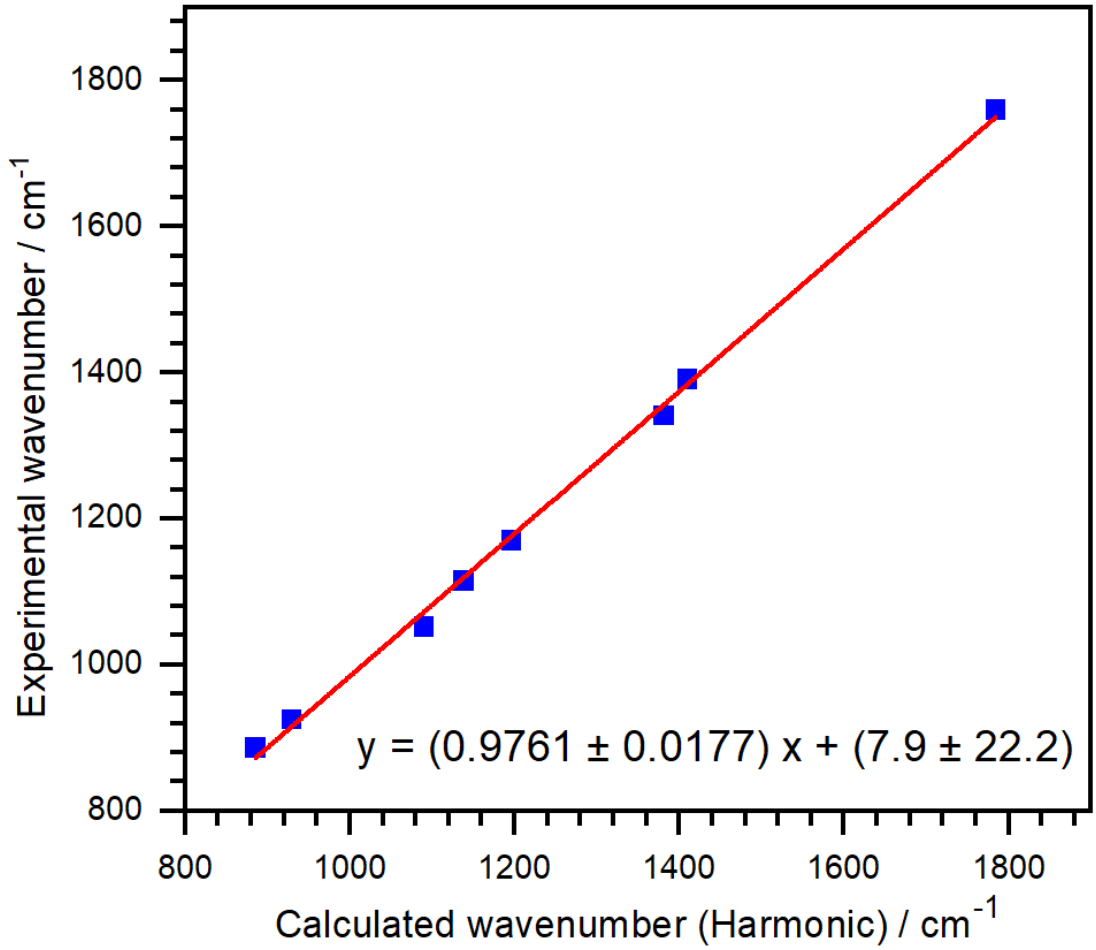


**Fig. S10** Linear fits of experimental wavenumbers vs. calculated harmonic vibrational wavenumbers of hydroperoxy methylformate (P5) in the spectral range 800−1900 $cm^{-1}$. The linear equation obtained on fitting the data was $y$ = (0.9761 ± 0.0177) $x$ + (7.9 ± 22.2); $y$ is the observed wavenumber and $x$ is the calculated harmonic vibrational wavenumber. Data are from reference 5.

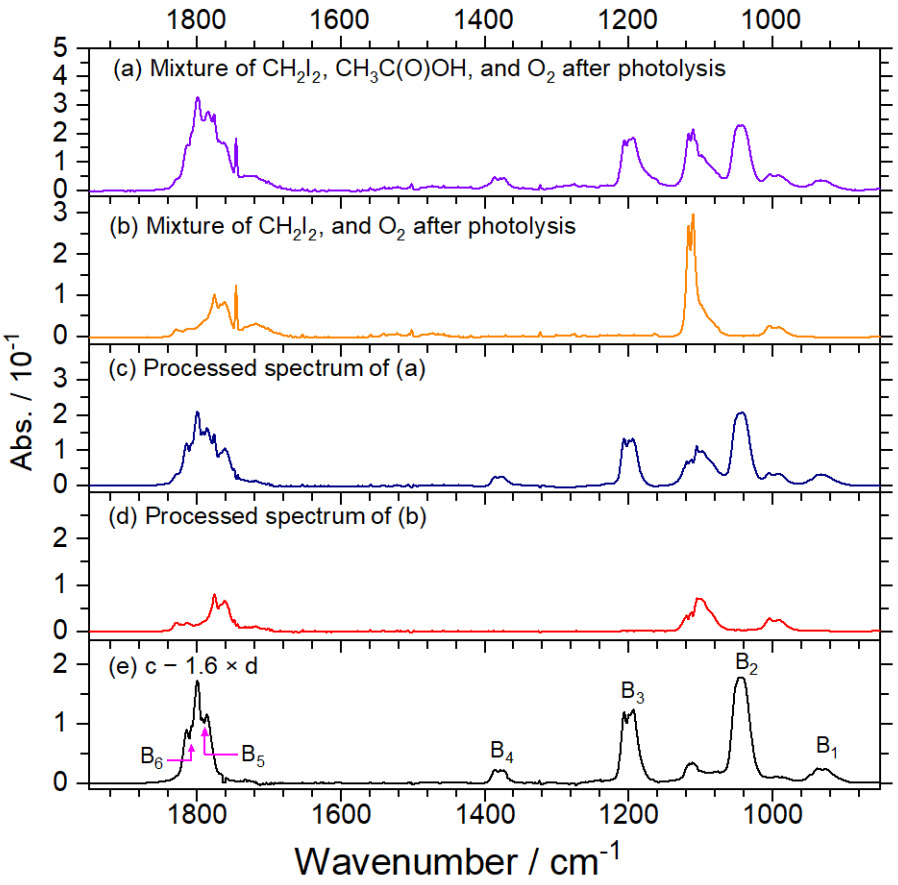


**Fig. S11** Comparison of IR spectra in static-cell experiments. (a) Spectrum of a mixture of $CH_2I_2/O_2/CH_3C(O)OH$ (0.147/41.0/0.025, $P_T$ = 41.2 Torr) recorded after photolysis at 308 nm (190 mJ, 10 Hz) for 1 min. (b) Spectrum of a mixture of $CH_2I_2/O_2$ (0.160/34.0, $P_T$ = 34.2 Torr) recorded after photolysis at 308 nm (190 mJ, 10 Hz) for 1 min. (c) Processed spectrum of (a); contributions of $H_2CO$, $CH_3C(O)OH$, and $CH_2I_2$ were removed. (d) Processed spectrum of (b); contributions of $H_2CO$, and $CH_2I_2$ were removed. (e) Difference spectrum of spectrum in (c) minus 1.6 times the spectrum in (d). Bands in group B are labeled. Resolution is 2 $cm^{-1}$.

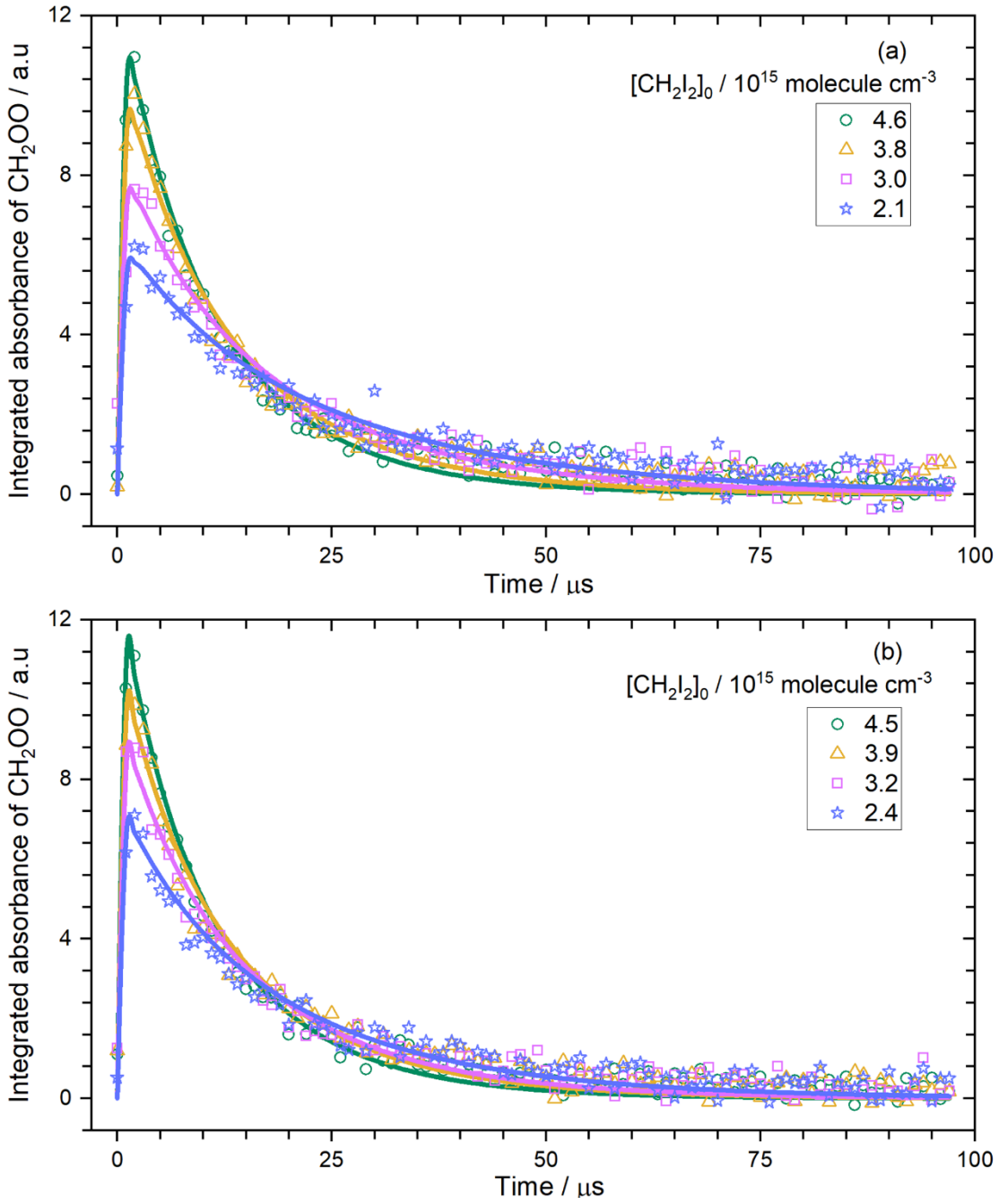


**Fig. S12** Representative temporal profiles of $CH_2OO$ (integrated in region 905–915 $cm^{-1}$) upon photolysis of a mixture of $CH_2I_2/O_2$ at 308 nm. (a) $O_2$ = 30 Torr and $CH_2I_2$ = 0.093–0.141 Torr and (b) $O_2$ = 40 Torr and $CH_2I_2$ = 0.098 – 0.144 Torr. The integrated spectral range for $CH_2OO$ is 905–915 $cm^{-1}$. The solid line represents the fitted temporal profile according to the model discussed in Section C.

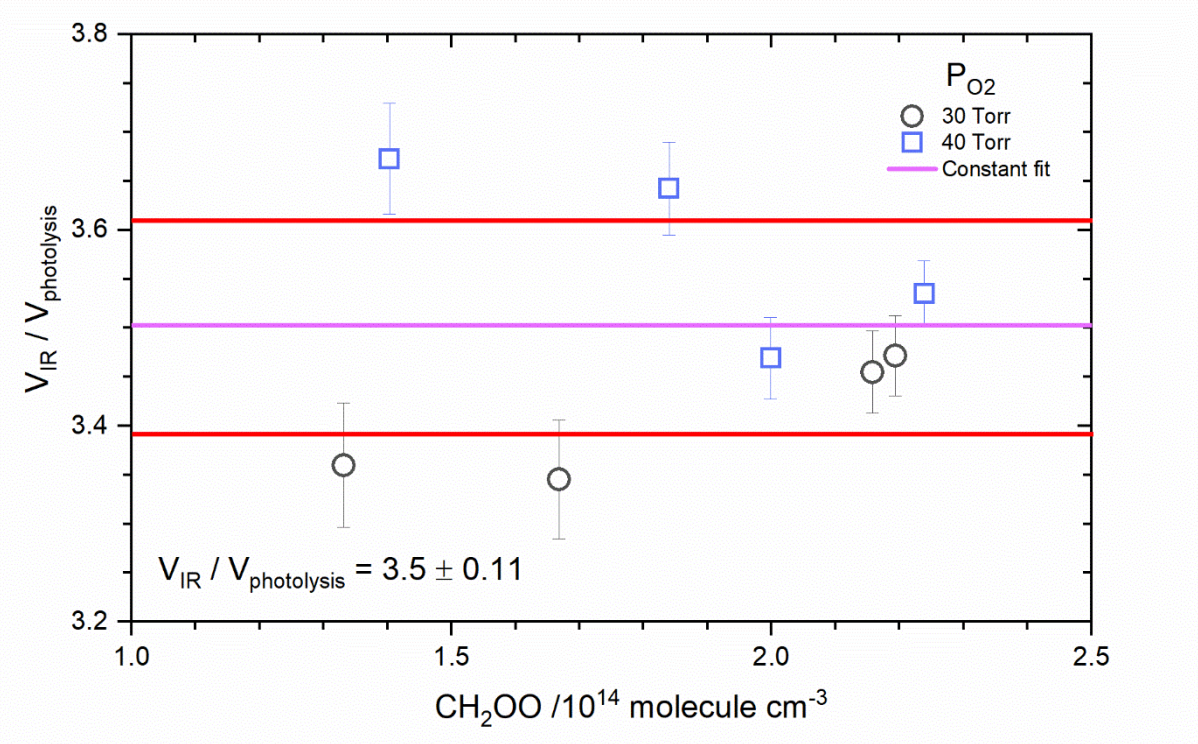


**Fig. S13** Measurements of volume ratio $V_{IR}/V_{photolysis}$ at varied $[CH_2OO]_0$. $[CH_2OO]_0$ was estimate at 0−5 μs period from the integrated band area and calculated IR intensity. Derivation is discussed in Section C. The purple line indicates the average value and the red lines represent the range of one standard deviation in fitting.

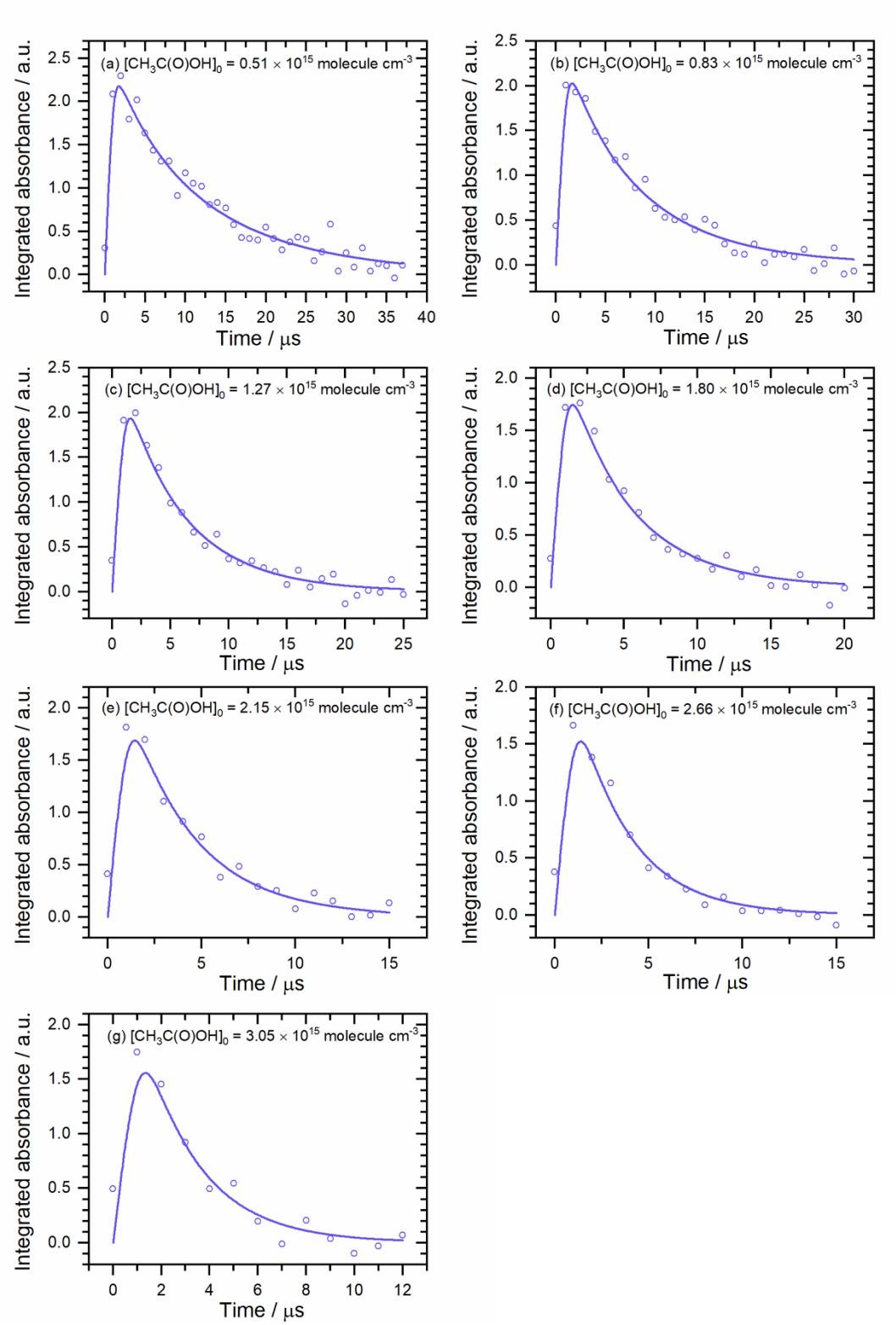


**Fig. S14** Representative temporal profiles for the rise and decay of $CH_2OO$ at various $[CH_3C(O)OH]_0$ in data set 3 (Table S21). Lines represent fitted temporal profiles according to the chemical model listed in (Table S20); see text.

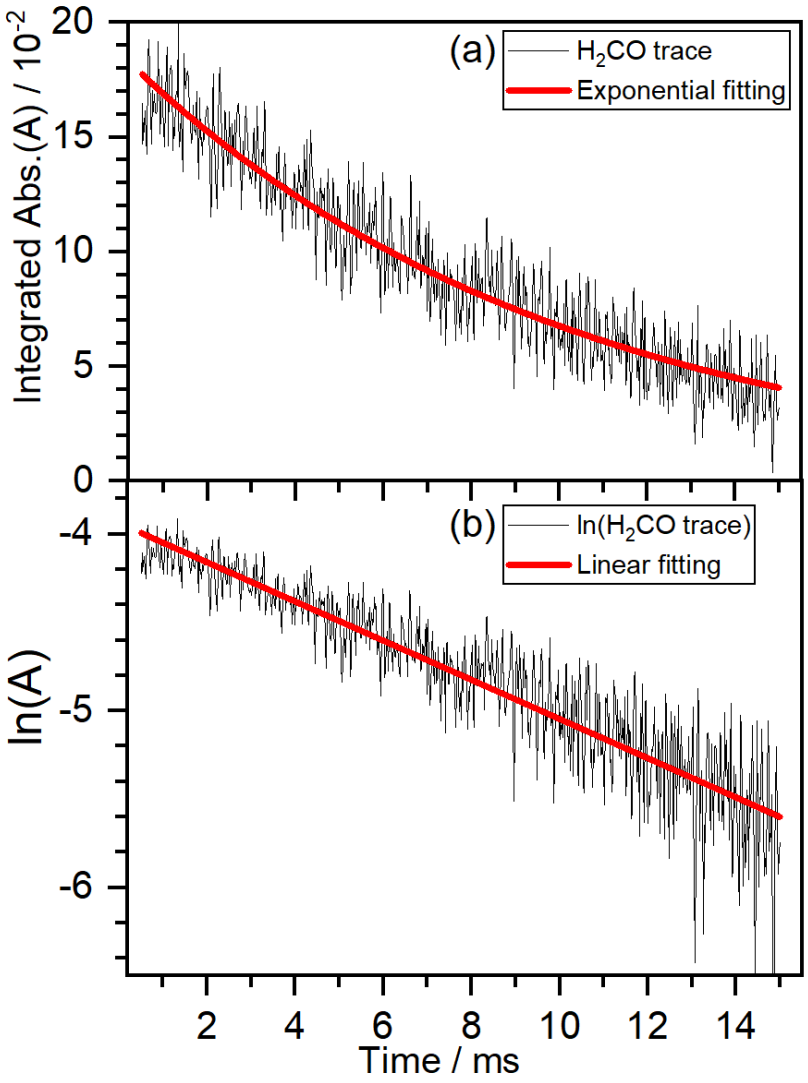


**Fig. S15** Temporal profiles for the decay of $H_2CO$ due to pumping. The solid red lines represent fitted temporal profiles. The data was obtained on integrating over the region 1742−1748 $cm^{-1}$ at temporal resolution 20 μs. The interference of HPMA in this region was eliminated by subtracting a factor 0.38 of HPMA integrated over 1240−1250 $cm^{-1}$. (a) Integrated absorbance of $H_2CO$ and single exponential fitting, (b) logarithmic of integrated absorbance of $H_2CO$ and linear fitting.

**References**


1 C. M. Western, *PGOPHER, A program for simulating rotational structure*, version 10.1.181, University of Bristol, U.K., http://pgopher.chm.bris.ac.uk.

2 T. J. Johnson, T. Masiello and S. W. Sharpe, *Atmos. Chem. Phys.*, 2006, **6**, 2581.

3 W.-L. Ting, C.-H. Chang, Y.-F. Lee, H. Matsui, Y.-P. Lee, and J. J.-M. Lin, *J. Chem. Phys.*, 2014, **141**, 104308.

4 Y.-T. Su, H.-Y. Lin, R. Putikam, H. Matsui, M. C. Lin, and Y.-P. Lee, *Nat. Chem.*, 2014, **6**, 477.

5 C. -A. Chung, J.W. Su, Y.-P. Lee, *Phys. Chem. Chem. Phys.*, 2019, **21**, 21445.

6 S. W. Sharpe, T. J. Johnson, R. L. Sams, P. M. Chu, G. C. Rhoderick and P. A. Johnson, *Appl. Spectrosc.*, 2004, **58**, 1452.

7 C. Mössinger, D. E. Shallcross and R. A. Cox, *J. Chem. Soc. Faraday Trans.*, 1998, **94**, 1391.

8 S. Enami, J. Ueda, M. Goto, Y. Nakano, S. Aloisio, S. Hashimoto and M. Kawasaki, *J. Phys. Chem. A*, 2004, **108**, 6347.

9 T. J. Gravestock, M. A. Blitz, W. J. Bloss and D. E. Heard, *Chem Phys Chem*, 2010, **11**, 3928.

10 R. Atkinson, D. L. Baulch, R. A. Cox, J. N. Crowley, R. F. Hampson, Jr., R. G. Hynes, M. E. Jenkin, M. J. Rossi and J. Troe, *Atmos. Chem. Phys.*, 2007, **7**, 981.